



## Did changes in atmospheric CO<sub>2</sub> coincide with latest Ordovician glacial–interglacial cycles?

Seth A. Young<sup>a,\*</sup>, Matthew R. Saltzman<sup>b</sup>, William I. Ausich<sup>b</sup>, André Desrochers<sup>c</sup>, Dimitri Kaljo<sup>d</sup>

<sup>a</sup> Department of Geological Sciences, Indiana University, Bloomington, IN 47405, USA

<sup>b</sup> Division of Geological Sciences, School of Earth Sciences, The Ohio State University, 125 S. Oval Mall, Columbus, OH 43210, USA

<sup>c</sup> Department of Earth Sciences, University of Ottawa, Ottawa, Ontario, Canada K1N 6N5

<sup>d</sup> Institute of Geology, Tallinn University of Technology, 5 Ehitajate tee, 19086 Tallinn, Estonia

### ARTICLE INFO

#### Article history:

Received 17 April 2009

Received in revised form 12 February 2010

Accepted 25 February 2010

Available online 2 March 2010

#### Keywords:

Late Ordovician

Carbon isotopes

Glaciations

Carbon dioxide

Estonia

Anticosti Island

### ABSTRACT

The Late Ordovician Hirnantian Stage (~444 million years ago) was one of three time periods during the past half billion years in which large continental glaciers formed over Earth's polar regions. The effects of this glaciation were far-reaching and coincided with one of the largest marine mass extinction events in Earth history. The cause of this ice age is uncertain, and a paradoxical association with evidence for high atmospheric CO<sub>2</sub> levels has been debated. Precise linkages between sea level, ice volume, and carbon isotope ( $\delta^{13}\text{C}_{\text{carb}}$  and  $\delta^{13}\text{C}_{\text{org}}$ ) proxy records of  $p\text{CO}_2$  have been poorly understood due in part to uncertainties in stratigraphic correlation and the interpretation of globally important sections. Although correlation difficulties remain, recent Hirnantian biostratigraphic studies now allow for improved correlations. Here we show that consistent trends in both  $\delta^{13}\text{C}_{\text{carb}}$  and  $\delta^{13}\text{C}_{\text{org}}$  from two well-dated stratigraphic sequences in Estonia and Anticosti Island, Canada coincide with changes in Late Ordovician (Hirnantian) climate as inferred from sea level and the extent of ice sheets. The integrated datasets are consistent with increasing  $p\text{CO}_2$  levels in response to ice-sheet expansion that reduced silicate weathering. Ultimately, the time period of elevated  $p\text{CO}_2$  levels is followed by geologic evidence of deglaciation.

© 2010 Elsevier B.V. All rights reserved.

### 1. Introduction

The Late Ordovician (Hirnantian) ice age is associated with one of the largest mass extinctions of marine organisms and a worldwide perturbation of the carbon cycle that produced a large positive carbon isotope ( $\delta^{13}\text{C}_{\text{carb}}$ ) excursion in marine carbonate rocks (Brenchley et al., 1994; Finney et al., 1999; Kump et al., 1999; Sutcliffe et al., 2000; Sheehan, 2001; Ghienne, 2003; Bergström et al., 2006; LaPorte et al., 2009). A new Ordovician sea surface temperature curve based on conodont-apatite  $\delta^{18}\text{O}$  (Trotter et al., 2008) supports an oceanic cooling event associated with the Hirnantian glaciation, along with a more prolonged cooling event through the Early–Middle Ordovician (Fig. 1). The early Katian Guttenberg  $\delta^{13}\text{C}$  excursion (GICE) that precedes the Hirnantian  $\delta^{13}\text{C}$  excursion may represent a cooling step (e.g., Patzkowsky et al., 1997; Pope and Steffen, 2003; Saltzman and Young, 2005), but this is not apparent in the paleotemperature of Trotter et al. (2008). Hypotheses that link the Hirnantian positive shift in  $\delta^{13}\text{C}_{\text{carb}}$  with climate and glaciation include enhanced oceanic circulation that increased productivity and burial of organic matter (Brenchley et al., 1994) or increased weathering of carbonates

exposed during eustatic drop (Kump et al., 1999). The two models differ in their predictions about the timing of changes in atmospheric  $p\text{CO}_2$  during glaciation and the  $\delta^{13}\text{C}_{\text{carb}}$  excursion. In the productivity model falling  $p\text{CO}_2$  and glaciation were induced by increased marine productivity that led to copious amounts of organic carbon (isotopically light;  $^{12}\text{C}$ ) being removed from the ocean–atmosphere system. Brenchley et al. (1994, 1995, 2003) equate the onset of the  $\delta^{13}\text{C}_{\text{carb}}$  excursion with falling sea level, lowering sea surface temperatures and  $p\text{CO}_2$  levels, ice-sheet expansion, and an initial phase of mass extinction. In contrast, the weathering hypothesis (Kump et al., 1999) proposes that  $p\text{CO}_2$  levels fell prior to the  $\delta^{13}\text{C}_{\text{carb}}$  excursion, perhaps resulting from increased silicate weatherability and resultant CO<sub>2</sub> consumption from exposed volcanic rocks associated with the Taconic Orogeny (Young et al., 2009). In this model  $p\text{CO}_2$  levels were low during initial ice-sheet development, but rose during glaciation as a result of a decrease in the percentage of silicate versus carbonate weathering. Hirnantian glacio-eustatic sea level fall exposed carbonate platforms and shifted riverine  $\delta^{13}\text{C}$  values positively yielding a contemporaneous increase of  $p\text{CO}_2$  levels and  $\delta^{13}\text{C}_{\text{carb}}$  values.

Proxy records of atmospheric  $p\text{CO}_2$  for the Late Ordovician ( $\delta^{13}\text{C}$  values from goethites; Yapp and Poths, 1992) are relatively coarse in resolution and difficult to correlate with marine sequences that contain sea-level records used to infer Hirnantian ice volume changes. Paired analysis of marine organic matter ( $\delta^{13}\text{C}_{\text{org}}$ ) and  $\delta^{13}\text{C}_{\text{carb}}$  also provides a

\* Corresponding author.

E-mail address: [seayoung@indiana.edu](mailto:seayoung@indiana.edu) (S.A. Young).

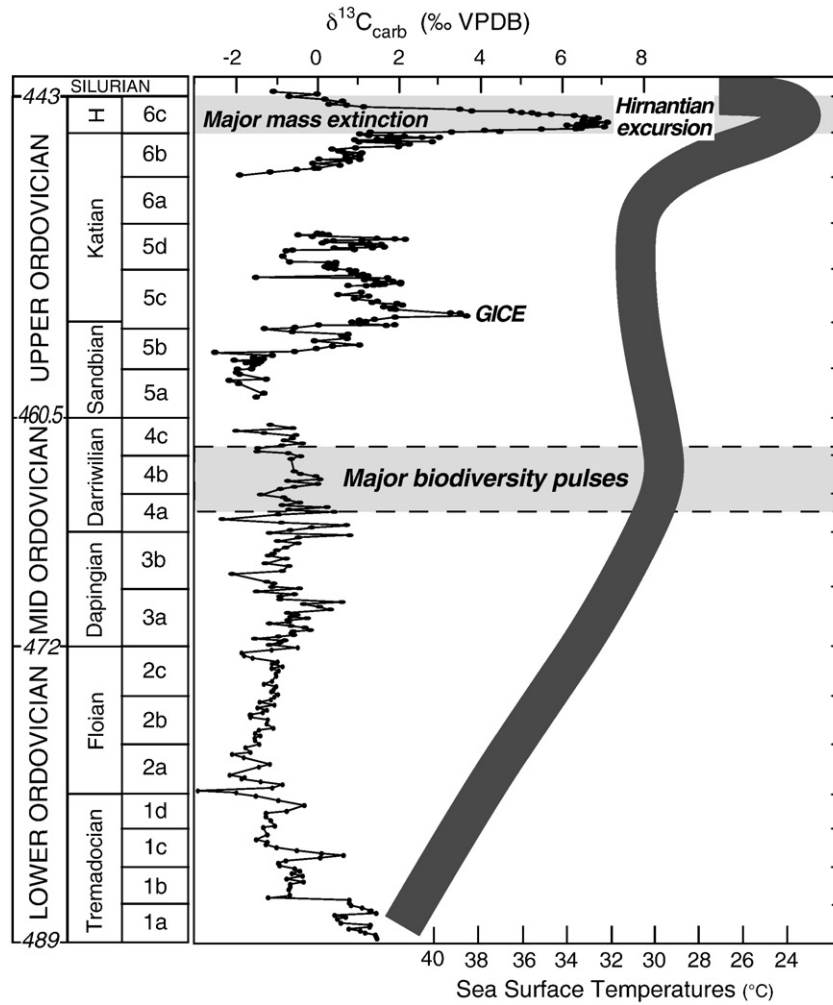


**Fig. 1.** Carbon isotopic ( $\delta^{13}\text{C}_{\text{carb}}$ ) variations in seawater through the Ordovician along with the conodont-apatite based tropical seawater temperature trend from Trotter et al. (2008). Ordovician  $\delta^{13}\text{C}_{\text{carb}}$  data replotted from Gao et al. (1996), Kump et al. (1999), Saltzman (2005), and Saltzman and Young (2005). Timescale (with new global stage names; H, Hirnantian), major biodiversity and extinction intervals are from Webby et al. (2004).

potential proxy for interpreting relative changes in atmospheric  $p\text{CO}_2$  (Hayes et al., 1999; Kump and Arthur, 1999; Kump et al., 1999). Obtaining globally representative  $\delta^{13}\text{C}_{\text{org}}$  values, however, remains a major challenge, particularly for bulk organic matter of ancient sediments that integrates many local variables (Bidigare et al., 1997; Popp et al., 1998; Joachimski et al., 2002). Use of paired analyses of marine  $\delta^{13}\text{C}_{\text{org}}$  and  $\delta^{13}\text{C}_{\text{carb}}$  as a  $p\text{CO}_2$  proxy thus relies on the degree to which similar trends are observed globally, and how strong an argument can be made that factors affecting  $\delta^{13}\text{C}$  on a local scale are unlikely to produce the same trend in widely separated oceanic regions (Francois et al., 1993; Bidigare et al., 1997; Popp et al., 1998; Pancost et al., 1999; Joachimski et al., 2002; Young et al., 2008). Specifically, the isotopic difference between paired  $\delta^{13}\text{C}_{\text{org}}$  and  $\delta^{13}\text{C}_{\text{carb}}$ , hereafter referred to as  $\Delta^{13}\text{C}$  ( $\Delta^{13}\text{C} = \delta^{13}\text{C}_{\text{carb}} - \delta^{13}\text{C}_{\text{org}}$ ), can only be used as a paleoatmospheric  $p\text{CO}_2$  proxy (Kump et al., 1999; Joachimski et al., 2002) when the overriding controls are changes in photosynthetic fractionation ( $\epsilon_p$ ) as a function of  $\text{CO}_{2(\text{aq})}$  concentrations.

Laboratory and field studies of modern marine phytoplankton have shown that  $\epsilon_p$  can also change as a function of cell growth rates or geometry (cell volume to surface area ratio) (Francois et al., 1993; Bidigare et al., 1997; Popp et al., 1998; Hayes et al., 1999; Joachimski et al., 2002). Furthermore, in addition to  $\epsilon_p$ , several other processes that also contribute to  $\Delta^{13}\text{C}$  may change through time, including: 1) temperature dependent fractionation between dissolved inorganic carbon (DIC) and  $\text{CO}_{2(\text{aq})}$  in seawater, and the fractionation between

DIC and precipitated carbonate minerals (e.g., calcite versus aragonite), and 2) organic matter sources, secondary biological fractionation (i.e., heterotrophy) and/or diagenesis (e.g., thermal maturation) (Hayes et al., 1999).

In order to produce meaningful high resolution  $\Delta^{13}\text{C}$  trends, the  $\delta^{13}\text{C}_{\text{org}}$  and  $\delta^{13}\text{C}_{\text{carb}}$  curves must ideally be constructed from the same carbonate-rich rock sequences, rather than separate shale versus carbonate successions, to avoid correlation problems that can hinder comparisons of the timing of changes (Kump and Arthur, 1999; Kump et al., 1999). Here, we present new paired analyses of  $\delta^{13}\text{C}_{\text{carb}}$  and  $\delta^{13}\text{C}_{\text{org}}$  from carbonate-rich sequences representing two low-latitude paleocontinents (Fig. 2). The  $\delta^{13}\text{C}$  data coupled with the sedimentary and biostratigraphic evidence from these and other key Hirnantian sections result in a revised interpretation of the timing and linkages among sea level, carbon cycling, and glaciation.

## 2. Background and geologic setting

Upper Ordovician carbonates from Estonia were deposited in an epicontinental marine platform setting on the paleocontinent of Baltica (Kaljo et al., 2001). The Kardla drill core from southern Estonia contains a thick (~100 m) Upper Ordovician sequence, deposited in a relatively deeper water shelf setting (i.e., the Livonian tongue; Kaljo et al., 2008). The upper Halliku, Kuldiga, Saldus, and lower Öhne formations were investigated from this drill core. Exposed on Anticosti Island, Quebec,

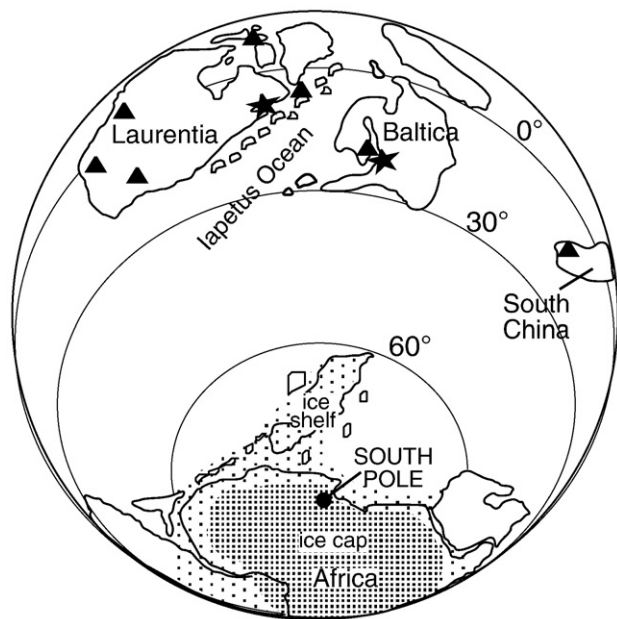


**Fig. 2.** Latest Ordovician paleogeographic map (after Cocks and Torsvik, 2002) with locations of the study areas (stars) on Anticosti Island, Quebec and Kardia drill core, Estonia shown. Previously studied Hirnantian sections (triangles) from Laurentia, Baltica, Scotland, and China are also shown (Brenchley et al., 1994; Underwood et al., 1997; Wang et al., 1997; Kump et al., 1999; Bergström et al., 2006; Melchin and Holmden, 2006; LaPorte et al., 2009).

Canada is a thick (~900 m with an additional 1200 m in subsurface), virtually undisturbed sequence of Upper Ordovician through Lower Silurian carbonates and siliciclastics, deposited in a carbonate shelf/ramp setting in a foreland basin on the western side of the Iapetus Ocean (Long, 2007). Outcroppings of the Vauréal, Ellis Bay, and lower Becscie (Fox Point member) formations from sections on western Anticosti Island were examined for this study.

Ordovician–Silurian boundary sections in both Estonia and Anticosti Island have been intensively examined, and the biostratigraphy of conodonts, graptolites, chitinozoans, and brachiopods facilitates global correlation (Fig. 3) (McCracken and Nowlan, 1986; Riva, 1988; Jin and Copper, 1997; Soufiane and Achab, 2000; Copper, 2001; Männik, 2001; Brenchley et al., 2003; Kaljo et al., 2008; Melchin, 2008; Achab et al., in press). Specifically, the presence of the chitinozoans *Belonechitina gamachiana* and *Spinachitina taugourdeui* (Soufiane and Achab, 2000; Achab et al., in press) in the Ellis Bay Formation (Anticosti Island) allows for precise correlation with sections from Estonia (Brenchley et al., 2003; Kaljo et al., 2008).

Although the chitinozoans mentioned here are useful for correlation between Estonia and Anticosti Island, the Hirnantian Global Stage boundaries are defined upon graptolite species from shale dominated sequences.

Recently the Global boundary Stratotype Section and Point (GSSP) for the base of the Hirnantian Stage was placed within the upper Wufeng Formation coinciding with the first occurrence of the graptolite *Normalograptus extraordinarius* at the Wangjiawan North section, China (Chen et al., 2006). Additionally, the Hirnantian Stage comprises two graptolite zones, with the lower being the *N. extraordinarius* biozone and the upper *N. persculptus* biozone. The *Amorphognathus ordovicicus* North Atlantic conodont Zone also extends through the Hirnantian Stage, interestingly *Noixodontus girardeauensis* is currently the only known conodont species limited to the Hirnantian, known from localities in Estonia and Midcontinent North America (Männik, 2001; Bergström et al., 2006; Kaljo et al., 2008). A unique brachiopod fauna (*Hirnantia* Fauna) has also been used to identify the Hirnantian Stage, although it has been demonstrated that certain species of this fauna are not confined to the Hirnantian Stage, ranging from upper *P. pacificus* through lower *P. acuminatus* graptolite biozones (e.g., Rong et al., 2002).

The other important fossil group widely used in latest Ordovician biostratigraphy is chitinozoans, and recently two schemes (A and B in Fig. 3) have emerged regarding integration of chitinozoan biozones established in carbonate-rich sequences (i.e., Estonia and Anticosti Island) with graptolite biozones established in shale dominated sections (e.g., Brenchley et al., 2003; Melchin et al., 2003). In the first scheme the *B. gamachiana* chitinozoan biozone is interpreted to be early Hirnantian, and thus correlative with the *N. extraordinarius* graptolite biozone, whereas the *S. taugourdeui* chitinozoan biozone is correlative with the late Hirnantian *N. persculptus* graptolite biozone (Melchin et al., 2003; Melchin and Holmden, 2006; Melchin 2008; Achab et al., in press). This scenario is supported by a reinterpretation of graptolites previously identified from Anticosti Island (Riva, 1988) and new collections suggesting that the upper half of the Ellis Bay Formation, including strata containing the chitinozoan *S. taugourdeui* (Soufiane and Achab, 2000a), is late Hirnantian (*N. persculptus* biozone; Melchin, 2008). However, graptolites from the Ellis Bay Formation appear to be controversial. “There is a lack of agreement among graptolite workers as to the identity of the graptolites first identified and figured by Riva (1988)” (Riva in Achab et al., in press). A lower Hirnantian age for the *B. gamachiana* biozone in the Ellis Bay Formation can only be “inferred” by Achab et al. (in press), and *B. gamachiana* also has a limited distribution in North America, only being reported from Anticosti Island thus far.

The second latest Ordovician biostratigraphic scheme interprets an early Hirnantian age for the *S. taugourdeui* chitinozoan biozone, placing it within the *N. extraordinarius* graptolite biozone, whereas

GLOBAL		FORMATIONS				GRAPTOLITE Biozones	Estonian Scheme A	Estonian Scheme B	CONODONT Biozones
Series	Stage	Nevada	Anticosti Is. Scheme A   Scheme B	Estonia	China		CHITINOZOAN Biozones	CHITINOZOAN Biozones	
UPPER ORDOVICIAN	HIRNANTIAN	Hanson Creek	Ellis Bay	Saldus	Lungmachi	<i>N. persculptus</i>	<i>C. scabra</i>		Noixodontus fauna
				Kuldiga	Kuanyinchiao Bed		<i>S. taugourdeui</i>	<i>C. scabra</i>	
					Wufeng	<i>N. extraordinarius</i>	<i>B. gamachiana</i>	<i>S. taugourdeui</i>	
	KAT- IAN		Vau-réal	Halliku		<i>P. pacificus</i>	<i>C. rugata</i>	<i>B. gamachiana</i>	Am. ordovicicus

**Fig. 3.** Stratigraphic chart showing late Katian and Hirnantian Formations from Nevada, Anticosti Island (Quebec, Canada), Estonia, and China along with graptolite, chitinozoan, and conodont biozonations. Note that biostratigraphic correlations for South China are from the Wangjiawan section (Chen et al., 2006). Estonian chitinozoan Scheme A is supported by the following previous work: Melchin et al. (2003), Melchin and Holmden (2006), Melchin (2008), and Achab et al. (in press). Estonian chitinozoan Scheme B is supported by the following previous studies: Brenchley et al. (2003), Bergström et al. (2006), Nõlvak et al. (2006), and Kaljo et al. (2008). Also note that Schemes A and B reflect the two differing chitinozoans biozonal schemes (i.e., Estonian Schemes A and B, respectively).

the preceding *B. gamachiana* chitinozoan biozone is correlative with upper *Paraorthograptus pacificus* or upper *Dicellograptus anceps* graptolite biozones of late Katian age (Brenchley et al., 2003; Bergström et al., 2006; Nölvak et al., 2006; Kaljo et al., 2008). The *S. taugourdeui* chitinozoan biozone has been recognized from strata containing *Hirnantia* Fauna brachiopods in Estonia (Kaljo et al., 2008), and now recently documented from the Hirnant Limestone, in Wales, which is the historical type area of the Hirnantian Stage (Vandenbroucke, 2008). Whereas the *B. gamachiana* chitinozoan biozone is

recognized through the ranges of *Hindella* and *Eospirigerina*, brachiopods of purported Hirnantian age (Jin and Copper, 1997, 2008; Copper, 2001), this age assignment remains controversial, as these brachiopods have been shown to occur in pre-Hirnantian strata elsewhere (e.g., Rong and Harper, 1988; Rong et al., 2002; Harper and Rong, 2008; Kaljo et al., 2008). Although these recent Hirnantian studies have contributed to the potential correlations of major biostratigraphic groups, it remains clear that only through further studies can a fully integrated global biostratigraphic framework

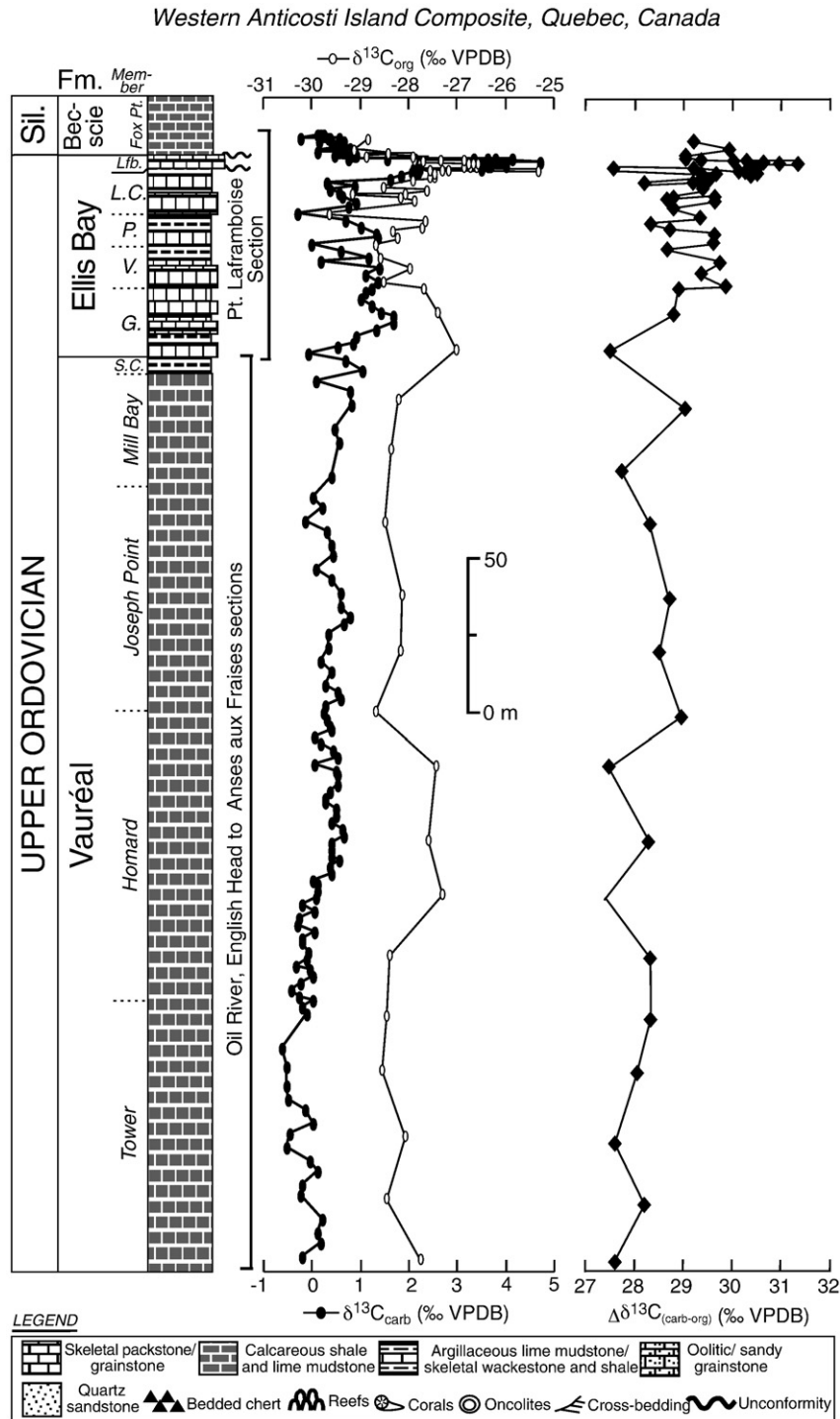


**Fig. 4.** Upper Ordovician to Lower Silurian  $\delta^{13}\text{C}_{\text{carb}}$  (filled circles) and  $\delta^{13}\text{C}_{\text{org}}$  (open circles) data for outcrop exposures on western Anticosti Island, Quebec, Canada. Composite of Ordovician surface exposures based upon previous conodont biostratigraphic studies (Nowlan and Barnes, 1981; McCracken and Barnes, 1981). Also plotted are  $\Delta^{13}\text{C}$  trends (diamonds; calculated as  $\delta^{13}\text{C}_{\text{carb}} - \delta^{13}\text{C}_{\text{org}}$ ), used as a proxy for relative changes in atmospheric  $p\text{CO}_2$ . Abbreviations: Schmitt Creek (S.C.), Grindstone (G.), Velleda (V.), Prinista (P.), Lousy Cove (L.C.), Laframboise (Lfb.).



emerge for the latest Ordovician (e.g., Delabroye and Vecoli, 2010). Whereas integration of biozones from these important fossil groups is paramount, testing the validity of differing biostratigraphic zonal schemes is beyond the scope of this paper.

### 3. Methods

The  $\delta^{13}\text{C}_{\text{carb}}$  and  $\delta^{13}\text{C}_{\text{org}}$  curves presented from the Estonia and Anticosti Island sections (Figs. 4 and 5) are constructed from micrites (i.e., lime mudstones) and bulk carbonates (grainstones where micritic matrix is absent), that underwent very low thermal alteration (Conodont Alteration Index: CAI  $\sim 1$ )  $< 50$ – $80$  °C (McCracken and Nowlan, 1986; Männik, 2001). Micrites and bulk carbonates have been previously demonstrated to record original  $\delta^{13}\text{C}_{\text{carb}}$  signatures from Late Ordovician seas (Long, 1993; Gao et al., 1996; Kaljo et al., 2001, 2007; LaPorte et al., 2009). Confidence in the ability of micrites and bulk carbonates to faithfully record pristine  $\delta^{13}\text{C}_{\text{carb}}$  signatures is based on the following arguments: 1) brachiopod calcite and micrite based  $\delta^{13}\text{C}_{\text{carb}}$  curves yield similar trends and isotopic values (e.g., Long, 1993; Brenchley et al., 1994, 2003; Bergström et al., 2006); 2) modeling studies indicate that  $\delta^{13}\text{C}_{\text{carb}}$  values of marine carbonates are largely rock-buffered during diagenesis (e.g., Banner and Hanson, 1990); and 3) many Paleozoic positive  $\delta^{13}\text{C}$  excursions have been documented in a wide variety of lithologies on several paleocontinents (e.g., Saltzman et al., 2000; Brenchley et al., 2003; Saltzman, 2002; among others). Well preserved organic matter may also occur in micrites and bulk carbonates for  $\delta^{13}\text{C}_{\text{org}}$  analyses (e.g., Patzkowsky et al., 1997; Pancost et al., 1999; Melchin and Holmden, 2006; LaPorte et al., 2009). Although alteration of primary  $\delta^{13}\text{C}_{\text{org}}$  values may occur (e.g., due to thermal alteration or oxidative loss of certain organic compounds) and may be more difficult to recognize than for  $\delta^{13}\text{C}_{\text{carb}}$ , we observe no systematic relationship between  $\delta^{13}\text{C}_{\text{org}}$  and wt.% TOC (see Tables 1 and 2) that might be expected if differential alteration of organic matter occurred in horizons that are lean versus relatively rich in organic carbon.

A water-based diamond-blade saw was used to produce thin-section billets that were then polished, and subsequently placed into an ultrasonic bath containing ultrapure (deionized, 18 M $\Omega$ ) water to remove surficial organic contaminants. Least altered components (following petrographic examination) were then preferentially

micro-drilled ( $\sim 1$  mg for  $\delta^{13}\text{C}_{\text{carb}}$  and  $\sim 1$  g for  $\delta^{13}\text{C}_{\text{org}}$ ) from thin-section billets.

Powders for  $\delta^{13}\text{C}_{\text{carb}}$  analyses were first roasted in a vacuum oven at 200 °C for 1 h to remove water and volatile organic contaminants. Then, 10–50  $\mu\text{g}$  of carbonate was reacted at 70 °C with 3–5 drops of anhydrous phosphoric acid for 180–300 s. Stable isotope values were obtained using a Finnigan Kiel-III carbonate preparation device directly coupled to the dual inlet of a Finnigan MAT 253 isotope ratio mass spectrometer in the Saskatchewan Isotope Laboratory at University of Saskatchewan. Sample powders for  $\delta^{13}\text{C}_{\text{org}}$  analyses were accurately weighed and acidified using 6 N HCl to remove carbonate minerals. Insoluble fractions were then repeatedly rinsed in ultrapure water and dried at 85 °C. Remaining residues were weighed and homogenized, and then loaded into tin capsules. Samples were combusted with a Costech Elemental Analyzer and the resulting  $\text{CO}_2$  gas analyzed for  $\delta^{13}\text{C}$  through a Finnigan Delta IV stable isotope ratio mass spectrometer under continuous flow using an open-split CONFLO III interface in the Stable Isotope Biogeochemistry Laboratory at The Ohio State University. Carbon isotope ratios presented here are reported in per mille notation relative to the Vienna Pee Dee Belemnite standard (‰ VPDB). Repeated measurements of the IAEA-NBS-19 standard were  $\pm 0.05$ ‰ and  $\pm 0.10$ ‰ for  $\delta^{13}\text{C}_{\text{carb}}$  and  $\delta^{18}\text{O}$  respectively through the course of this study. Additionally, multiple analyses of IAEA-CH7 standard were  $\pm 0.15$ ‰ for  $\delta^{13}\text{C}_{\text{org}}$ , and  $\pm 1.0$ ‰ for  $\delta^{13}\text{C}$  (1 standard deviation). Weight percent of total organic carbon (TOC) in samples is determined by comparison of voltages for the ion beam intensities of masses 44, 45, and 46  $\text{CO}_2^+$  between our samples and known wt.% carbon of the gravimetric standard Acetanilide.

### 4. Results

#### 4.1. Anticosti Island, Quebec, Canada

The Vauréal Formation was sampled continuously from outcrops along the Oil River (Tower and Homard members), and along tidal flat exposures from English Head to Anses aux Fraises (Homard, Joseph Point, Mill Bay, and Schmitt Creek members) (Nowlan and Barnes, 1981). Interbedded lime mudstones and calcareous shales are the dominant lithologies, with sparse packstone/grainstone occurrences from these outcrops. The Ellis Bay and Becscie formations were sampled from exposures near Pointe Laframboise (McCracken and

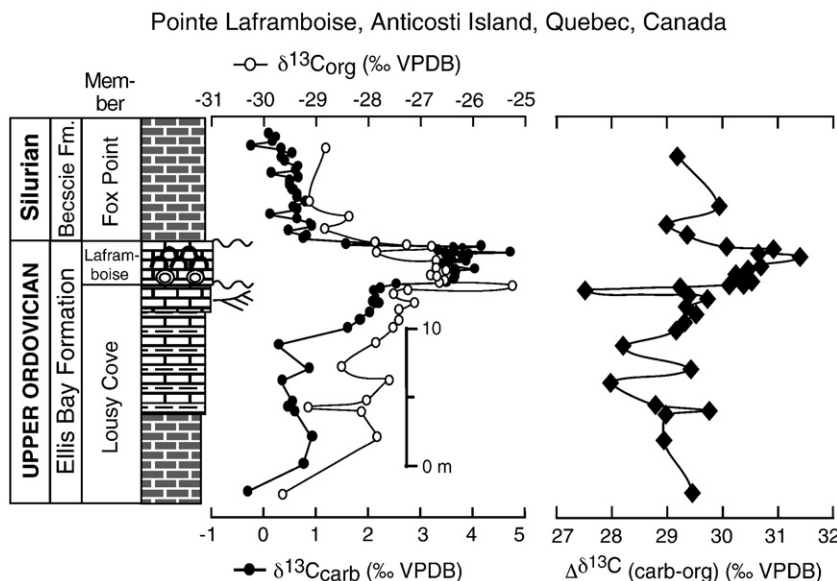


Fig. 5. Upper Ordovician to Lower Silurian  $\delta^{13}\text{C}_{\text{carb}}$  and  $\delta^{13}\text{C}_{\text{org}}$  trends for Pointe Laframboise, western Anticosti Island, Quebec, Canada. For the lithologic legend refer to Fig. 4 and also note that the scales for  $\delta^{13}\text{C}_{\text{carb}}$  and  $\delta^{13}\text{C}_{\text{org}}$  are below and above the data plots, respectively.  $\Delta^{13}\text{C}$  trends are also plotted, and used as a proxy for relative changes in atmospheric  $p\text{CO}_2$ . Note the presence of two unconformities capping the Lousy Cove and Laframboise members.

**Table 1**

Stable isotope data, western Anticosti Island, Quebec, Canada.

Meters <sup>a</sup>	$\delta^{13}\text{C}_{\text{carb}}$	$\delta^{18}\text{O}$	$\delta^{13}\text{C}_{\text{org}}$	TOC <sup>b</sup>	Formation	Member	Chitinozoan zone
0	−0.21	−4.62	−27.77	0.06	Vauréal	Tower	<i>H. normalis</i>
4	0.19	−4.71			Vauréal	Tower	<i>H. normalis</i>
8	0.13	−4.68			Vauréal	Tower	<i>H. normalis</i>
12	0.22	−4.41			Vauréal	Tower	<i>H. normalis</i>
20	−0.23	−4.81	−28.45	0.03	Vauréal	Tower	<i>H. normalis</i>
24	−0.19	−4.42			Vauréal	Tower	<i>H. normalis</i>
28	0.12	−4.13			Vauréal	Tower	<i>H. normalis</i>
32	−0.04	−4.41			Vauréal	Tower	<i>H. normalis</i>
36	−0.51	−4.70			Vauréal	Tower	<i>H. normalis</i>
40	−0.46	−5.04	−28.09	0.53	Vauréal	Tower	<i>H. normalis</i>
44	0.01	−4.92			Vauréal	Tower	<i>H. normalis</i>
48	−0.14	−5.00			Vauréal	Tower	<i>H. normalis</i>
52	−0.49	−4.27			Vauréal	Tower	<i>H. normalis</i>
56	−0.51	−5.08			Vauréal	Tower	<i>H. normalis</i>
62.5	−0.51	−4.54	−28.57	0.05	Vauréal	Tower	<i>H. normalis</i>
69	−0.63	−5.10			Vauréal	Homard	<i>H. normalis</i>
80	−0.09	−3.89	−28.45	0.06	Vauréal	Homard	<i>H. normalis</i>
82	−0.21	−4.86			Vauréal	Homard	<i>H. normalis</i>
84	0.02	−4.21			Vauréal	Homard	<i>H. normalis</i>
86	−0.26	−4.30			Vauréal	Homard	<i>H. normalis</i>
88	−0.42	−4.50			Vauréal	Homard	<i>H. normalis</i>
90	−0.24	−4.36			Vauréal	Homard	<i>H. normalis</i>
92	0.02	−4.39			Vauréal	Homard	<i>H. normalis</i>
94	−0.04	−4.72			Vauréal	Homard	<i>H. normalis</i>
96	−0.34	−4.37			Vauréal	Homard	<i>H. normalis</i>
98	−0.09	−4.31			Vauréal	Homard	<i>H. normalis</i>
100	−0.06	−4.03	−28.41	0.03	Vauréal	Homard	<i>H. normalis</i>
103	−0.21	−3.93			Vauréal	Homard	<i>H. normalis</i>
105	−0.21	−4.21			Vauréal	Homard	<i>H. normalis</i>
107	0.04	−4.16			Vauréal	Homard	<i>H. normalis</i>
109	−0.30	−4.22			Vauréal	Homard	<i>H. normalis</i>
111	−0.27	−5.01			Vauréal	Homard	<i>H. normalis</i>
114	0.05	−3.82			Vauréal	Homard	<i>H. normalis</i>
116	−0.21	−4.72			Vauréal	Homard	<i>H. normalis</i>
118	0.10	−4.45			Vauréal	Homard	<i>H. normalis</i>
120	0.13	−4.41	−27.30	0.04	Vauréal	Homard	<i>H. normalis</i>
122	0.11	−4.27			Vauréal	Homard	<i>H. normalis</i>
124	0.02	−4.19			Vauréal	Homard	<i>H. normalis</i>
126	0.40	−4.04			Vauréal	Homard	<i>H. normalis</i>
128	0.37	−3.92			Vauréal	Homard	<i>H. normalis</i>
130	0.55	−4.05			Vauréal	Homard	<i>H. normalis</i>
132	0.42	−4.54			Vauréal	Homard	<i>H. normalis</i>
134	0.41	−4.71			Vauréal	Homard	<i>H. normalis</i>
136	0.39	−4.53			Vauréal	Homard	<i>H. normalis</i>
138	0.67	−3.91	−27.61	0.04	Vauréal	Homard	<i>H. normalis</i>
140	0.63	−3.96			Vauréal	Homard	<i>H. normalis</i>
143	0.39	−3.89			Vauréal	Homard	<i>H. normalis</i>
145	0.50	−4.11			Vauréal	Homard	<i>H. normalis</i>
147	0.51	−4.29			Vauréal	Homard	<i>H. normalis</i>
149	0.27	−4.45			Vauréal	Homard	<i>H. normalis</i>
151	0.27	−4.14			Vauréal	Homard	<i>H. normalis</i>
153	0.36	−5.07			Vauréal	Homard	<i>H. normalis</i>
155	0.52	−4.29			Vauréal	Homard	<i>H. normalis</i>
158	0.54	−3.87			Vauréal	Homard	<i>H. normalis</i>
160	0.49	−4.10			Vauréal	Homard	<i>H. normalis</i>
162	0.07	−4.50	−27.44	0.01	Vauréal	Homard	<i>H. normalis</i>
164	0.53	−4.27			Vauréal	Homard	<i>H. normalis</i>
166	0.43	−4.08			Vauréal	Homard	<i>H. normalis</i>
169	0.19	−4.23			Vauréal	Homard	<i>H. normalis</i>
171	0.07	−4.51			Vauréal	Homard	<i>H. normalis</i>
173	0.40	−3.76			Vauréal	Homard	<i>H. normalis</i>
174	0.38	−3.86			Vauréal	Joseph Point	<i>H. crickmayi</i>
177	0.30	−3.93			Vauréal	Joseph Point	<i>H. crickmayi</i>
179	0.26	−3.93	−28.70	0.03	Vauréal	Joseph Point	<i>H. crickmayi</i>
181	0.27	−4.35			Vauréal	Joseph Point	<i>H. crickmayi</i>
183	0.61	−3.79			Vauréal	Joseph Point	<i>H. crickmayi</i>
185	0.52	−3.52			Vauréal	Joseph Point	<i>H. crickmayi</i>
188	0.28	−3.94			Vauréal	Joseph Point	<i>H. crickmayi</i>
192	0.39	−4.15			Vauréal	Joseph Point	<i>H. crickmayi</i>
196	0.17	−4.14			Vauréal	Joseph Point	<i>H. crickmayi</i>
200	0.34	−3.75	−28.17	0.03	Vauréal	Joseph Point	<i>H. crickmayi</i>
204	0.35	−3.70			Vauréal	Joseph Point	<i>H. crickmayi</i>
208	0.65	−3.57			Vauréal	Joseph Point	<i>H. crickmayi</i>
210	0.80	−4.37			Vauréal	Joseph Point	<i>H. crickmayi</i>
214	0.60	−3.82			Vauréal	Joseph Point	<i>H. crickmayi</i>

(continued on next page)

Table 1 (continued)

Meters <sup>a</sup>	$\delta^{13}\text{C}_{\text{carb}}$	$\delta^{18}\text{O}$	$\delta^{13}\text{C}_{\text{org}}$	TOC <sup>b</sup>	Formation	Member	Chitinozoan zone
218	0.59	−3.58	−28.15	0.05	Vauréal	Joseph Point	<i>H. crickmayi</i>
222	0.42	−3.92			Vauréal	Joseph Point	<i>H. crickmayi</i>
226	0.10	−3.60			Vauréal	Joseph Point	<i>H. crickmayi</i>
230	0.44	−5.11			Vauréal	Joseph Point	<i>H. crickmayi</i>
234	0.41	−3.89			Vauréal	Joseph Point	<i>H. crickmayi</i>
238	0.31	−3.62			Vauréal	Joseph Point	<i>H. crickmayi</i>
242	−0.14	−3.83	−28.48	0.05	Vauréal	Joseph Point	<i>H. crickmayi</i>
246	0.22	−3.56			Vauréal	Joseph Point	<i>H. crickmayi</i>
250	0.01	−4.20			Vauréal	Joseph Point	<i>H. crickmayi</i>
256	0.39	−4.01			Vauréal	Joseph Point	<i>H. crickmayi</i>
260	−0.64	−4.18	−28.41	0.08	Vauréal	Mill Bay	<i>H. crickmayi</i>
268	0.56	−3.54			Vauréal	Mill Bay	<i>H. crickmayi</i>
272	0.47	−3.87			Vauréal	Mill Bay	<i>H. crickmayi</i>
280	0.82	−3.46	−28.21	0.08	Vauréal	Mill Bay	<i>H. crickmayi</i>
284	0.78	−3.46			Vauréal	Mill Bay	<i>H. crickmayi</i>
288	0.08	−3.44			Vauréal	Mill Bay	<i>H. crickmayi</i>
291.1	1.03	−3.72			Vauréal	Schmitt Creek	<i>H. crickmayi</i>
294.5	0.69	−3.58			Vauréal	Schmitt Creek	<i>H. crickmayi</i>
296.5	−0.07	−3.91			Ellis Bay	Grindstone	<i>B. gamachiana</i>
298.5	0.53	−4.30	−27.01	0.05	Ellis Bay	Grindstone	<i>B. gamachiana</i>
300.5	0.85	−3.71			Ellis Bay	Grindstone	<i>B. gamachiana</i>
302.5	0.91	−3.74			Ellis Bay	Grindstone	<i>B. gamachiana</i>
304.5	1.34	−3.32			Ellis Bay	Grindstone	<i>B. gamachiana</i>
306.5	1.69	−3.52			Ellis Bay	Grindstone	<i>B. gamachiana</i>
308.5	1.68	−3.30			Ellis Bay	Grindstone	<i>B. gamachiana</i>
310.5	1.43	−3.60	−27.39	0.06	Ellis Bay	Grindstone	<i>B. gamachiana</i>
312.5	1.24	−3.03			Ellis Bay	Grindstone	<i>B. gamachiana</i>
314.5	1.00	−4.06			Ellis Bay	Grindstone	<i>B. gamachiana</i>
316.5	1.12	−3.96			Ellis Bay	Grindstone	<i>B. gamachiana</i>
318.5	1.25	−3.46			Ellis Bay	Velleda	<i>B. gamachiana</i>
320.5	1.37	−3.70			Ellis Bay	Velleda	<i>B. gamachiana</i>
322.5	1.12	−3.32			Ellis Bay	Velleda	<i>B. gamachiana</i>
324.5	1.41	−4.53	−27.97	0.04	Ellis Bay	Velleda	<i>B. gamachiana</i>
326.5	0.18	−2.67			Ellis Bay	Velleda	<i>B. gamachiana</i>
328.5	1.16	−3.72			Ellis Bay	Velleda	<i>B. gamachiana</i>
330.5	0.59	−3.47			Ellis Bay	Velleda	<i>B. gamachiana</i>
332.5	−0.02	−3.31			Ellis Bay	Velleda	<i>B. gamachiana</i>
334.5	1.36	−3.47			Ellis Bay	Prinsta	<i>B. gamachiana</i>
336.5	1.32	−3.42	−28.32	0.07	Ellis Bay	Prinsta	<i>B. gamachiana</i>
338.5	1.02	−3.59			Ellis Bay	Prinsta	<i>B. gamachiana</i>
340.5	0.69	−3.58			Ellis Bay	Lousy Cove	<i>B. gamachiana</i>
342.5	−0.29	−3.81	−29.63	0.09	Ellis Bay	Lousy Cove	<i>B. gamachiana</i>
344.5	0.77	−3.70			Ellis Bay	Lousy Cove	<i>B. gamachiana</i>
346.5	0.93	−4.26	−27.87	0.10	Ellis Bay	Lousy Cove	<i>B. gamachiana</i>
348.5	0.62	−3.71	−28.18	0.09	Ellis Bay	Lousy Cove	<i>B. gamachiana</i>
348.8	0.48	−3.32	−29.16	0.07	Ellis Bay	Lousy Cove	<i>B. gamachiana</i>
349.1	0.57	−3.86	−28.09	0.08	Ellis Bay	Lousy Cove	<i>B. gamachiana</i>
350.6	0.36	−4.12	−27.64	0.06	Ellis Bay	Lousy Cove	<i>B. gamachiana</i>
351.5	0.87	−3.71	−28.54	0.06	Ellis Bay	Lousy Cove	<i>B. gamachiana</i>
353.3	0.30	−3.68	−27.92	0.07	Ellis Bay	Lousy Cove	<i>B. gamachiana</i>
354.5	1.62	−2.69	−27.56	0.05	Ellis Bay	Lousy Cove	<i>S. tougourdeani</i>
355.1	1.84	−2.83	−27.46	0.08	Ellis Bay	Lousy Cove	<i>S. tougourdeani</i>
355.7	2.05	−2.65	−27.48	0.11	Ellis Bay	Lousy Cove	<i>S. tougourdeani</i>
356.3	2.19	−3.51	−27.17	0.32	Ellis Bay	Lousy Cove	<i>S. tougourdeani</i>
356.6	2.09	−3.29			Ellis Bay	Lousy Cove	<i>S. tougourdeani</i>
356.9	2.16	−3.49	−27.56	0.06	Ellis Bay	Lousy Cove	<i>S. tougourdeani</i>
357.2	2.10	−3.81	−27.30	0.03	Ellis Bay	Lousy Cove	<i>S. tougourdeani</i>
357.5	2.23	−3.63	−25.32	0.01	Ellis Bay	Lousy Cove	<i>S. tougourdeani</i>
357.8	2.54	−4.03	−26.70	0.03	Ellis Bay	Lousy Cove	<i>S. tougourdeani</i>
357.9	3.49	−2.12	−26.60	0.06	Ellis Bay	Laframboise	???
358.1	3.63	−1.88	−26.72	0.03	Ellis Bay	Laframboise	???
358.3	3.65	−2.48	−26.86	0.04	Ellis Bay	Laframboise	???
358.5	3.65	−2.18	−26.66	0.05	Ellis Bay	Laframboise	???
358.7	3.69	−2.64	−26.58	0.03	Ellis Bay	Laframboise	???
358.8	3.66	−2.90	−26.76	0.02	Ellis Bay	Laframboise	???
358.9	4.02	−2.37			Ellis Bay	Laframboise	???
359.2	3.43	−3.49			Ellis Bay	Laframboise	???
359.3	3.34	−3.47			Ellis Bay	Laframboise	???
359.4	3.86	−2.50	−26.77	0.03	Ellis Bay	Laframboise	???
359.5	3.54	−3.01			Ellis Bay	Laframboise	???
359.6	3.58	−3.36			Ellis Bay	Laframboise	???
359.7	3.87	−3.02			Ellis Bay	Laframboise	???
359.8	3.80	−2.47			Ellis Bay	Laframboise	???
359.9	3.91	−2.49			Ellis Bay	Laframboise	???
360	3.47	−2.43	−27.88	0.01	Ellis Bay	Laframboise	???
360.1	4.70	−1.92			Ellis Bay	Laframboise	???

Table 1 (continued)

Meters <sup>a</sup>	$\delta^{13}\text{C}_{\text{carb}}$	$\delta^{18}\text{O}$	$\delta^{13}\text{C}_{\text{org}}$	TOC <sup>b</sup>	Formation	Member	Chitinozoan zone
360.2	3.33	−3.43			Ellis Bay	Laframboise	???
360.3	3.63	−3.06			Ellis Bay	Laframboise	???
360.4	3.78	−2.05	−26.85	0.03	Ellis Bay	Laframboise	???
360.5	4.14	−2.06			Ellis Bay	Laframboise	???
360.6	3.63	−2.89	−27.33	0.02	Ellis Bay	Laframboise	???
360.7	1.57	−3.26			Becsie	Fox Point	<i>A. ellisbayensis</i>
360.8	2.14	−4.05	−27.91	0.03	Becsie	Fox Point	<i>A. ellisbayensis</i>
361.1	0.76	−3.98			Becsie	Fox Point	<i>A. ellisbayensis</i>
361.4	0.83	−4.69			Becsie	Fox Point	<i>A. ellisbayensis</i>
361.7	0.48	−3.88	−28.87	0.01	Becsie	Fox Point	<i>A. ellisbayensis</i>
362	0.93	−3.57			Becsie	Fox Point	<i>A. ellisbayensis</i>
362.3	0.87	−3.74			Becsie	Fox Point	<i>A. ellisbayensis</i>
362.6	0.65	−3.27	−28.42	0.04	Becsie	Fox Point	<i>A. ellisbayensis</i>
362.9	0.13	−3.75			Becsie	Fox Point	<i>P. nodifera</i>
363.2	0.64	−3.45			Becsie	Fox Point	<i>P. nodifera</i>
363.5	0.57	−3.78			Becsie	Fox Point	<i>P. nodifera</i>
363.8	0.80	−3.55	−29.14	0.04	Becsie	Fox Point	<i>P. nodifera</i>
364.1	0.64	−3.50			Becsie	Fox Point	<i>P. nodifera</i>
364.4	0.65	−3.47			Becsie	Fox Point	<i>P. nodifera</i>
364.7	0.56	−3.63			Becsie	Fox Point	<i>P. nodifera</i>
365	0.51	−3.70			Becsie	Fox Point	<i>P. nodifera</i>
365.3	0.50	−3.83			Becsie	Fox Point	<i>P. nodifera</i>
365.6	0.67	−3.52			Becsie	Fox Point	<i>P. nodifera</i>
365.9	0.15	−3.83			Becsie	Fox Point	<i>P. nodifera</i>
366.2	0.61	−3.63			Becsie	Fox Point	<i>P. nodifera</i>
366.5	0.67	−3.63			Becsie	Fox Point	<i>P. nodifera</i>
366.8	0.41	−4.08			Becsie	Fox Point	<i>P. nodifera</i>
367.1	0.38	−3.84			Becsie	Fox Point	<i>P. nodifera</i>
367.4	0.55	−3.55			Becsie	Fox Point	<i>P. nodifera</i>
367.7	0.33	−3.85	−28.85	0.06	Becsie	Fox Point	<i>P. nodifera</i>
368	−0.24	−3.75			Becsie	Fox Point	<i>P. nodifera</i>
368.3	0.17	−3.65			Becsie	Fox Point	<i>P. nodifera</i>
368.6	0.24	−3.40			Becsie	Fox Point	<i>P. nodifera</i>
368.9	0.11	−3.88			Becsie	Fox Point	<i>P. nodifera</i>

<sup>a</sup> Composite begins with Vauéal Fm. measured along the Oil River, continuing with tidal flat exposures at English Head to Anses aux Fraises. Ellis Bay and Becsie formations measured at Pointe Laframboise section.

<sup>b</sup> Fractional weight of total organic carbon in each sample.

Barnes, 1981; Jin and Copper, 1997), with carbonate facies being more diverse in the Ellis Bay Formation, ranging from bioturbated mudstones to oncolitic packstones and reefal boundstones.

Values of  $\delta^{13}\text{C}_{\text{carb}}$  from the Vauréal Formation at the mouth of the Oil River begin near 0.0‰ with little fluctuation ( $\leq 0.5\%$ ) through the Tower and Homard members (Fig. 4).  $\delta^{13}\text{C}_{\text{org}}$  values in the Vauréal Formation begin at  $-27.8\%$  and also show little variation through the Vauréal Formation ( $\leq 0.5\%$ ). Small-scale fluctuations in  $\delta^{13}\text{C}_{\text{carb}}$  values, ranging from  $-0.3\%$  to  $+1.7\%$ , begin in the uppermost Vauréal Formation (Schmitt Creek Member) and continue into the Ellis Bay Formation.  $\delta^{13}\text{C}_{\text{org}}$  values also show fluctuations ranging from  $-28.5\%$  to  $-27.0\%$  in the Grindstone through Prinstam members. The upper Ellis Bay Formation (lower Lousy Cove Member) records relatively steady  $\delta^{13}\text{C}_{\text{carb}}$  and  $\delta^{13}\text{C}_{\text{org}}$  values ( $\sim 0$  to  $+1\%$ ,  $-29.6$  to  $-28.0\%$  respectively) before a positive shift in the upper Lousy Cove Member (Fig. 5). The overlying Laframboise reefs record a sharp increase in  $\delta^{13}\text{C}_{\text{carb}}$  ( $+3.3$  to  $+4.7\%$ ) and declining  $\delta^{13}\text{C}_{\text{org}}$  values ( $-28\%$  to  $-26.6\%$ ). Values return to a pre-excursion baseline in the overlying Becsie Formation on Anticosti Island.

#### 4.2. Kardla drill core, Estonia

A continuous series of samples was collected from formations spanning the *C. rugata* through *S. fragilis* Chitinozoan Biozones within the Kardla drill core (Kaljo et al., 2001; Brenchley et al., 2003). The Halliku, Kuldiga, Öhne formations are predominantly interbedded lime mudstones and calcareous shales, with oolitic and sandy pack- to grainstones occurring in the Saldus Formation.  $\delta^{13}\text{C}_{\text{carb}}$  and  $\delta^{13}\text{C}_{\text{org}}$  remain relatively steady in the upper Halliku Formation ( $+0.8$  to  $+1.1\%$ ,  $-29.5$  to  $-28.8\%$  respectively) before shifting to more positive values in the overlying Bernati Member of the Kuldiga

Formation (Fig. 6). Peak  $\delta^{13}\text{C}_{\text{carb}}$  and  $\delta^{13}\text{C}_{\text{org}}$  values ( $+6.8\%$  and  $-25.4\%$ , respectively) are recorded in the Edole Member of the Kuldiga Formation.  $\delta^{13}\text{C}$  values remain elevated in the oolitic Saldus Formation, with pre-excursion  $\delta^{13}\text{C}$  values returning in the lowermost Öhne Formation.

## 5. Discussion

### 5.1. Correlations with other Hirnantian $\delta^{13}\text{C}_{\text{carb}}$ and $\delta^{13}\text{C}_{\text{org}}$ curves

Our paired analyses from Estonia and Anticosti Island demonstrate excursions in  $\delta^{13}\text{C}_{\text{carb}}$  and  $\delta^{13}\text{C}_{\text{org}}$  from these Hirnantian sections for the first time. These  $\delta^{13}\text{C}_{\text{org}}$  trends are consistent with a positive shift in  $\delta^{13}\text{C}_{\text{org}}$  previously documented from other Hirnantian sections (Underwood et al., 1997; Wang et al., 1997; Chen et al., 2006; Zhang et al., 2009), and with the previously well-documented large positive shift in  $\delta^{13}\text{C}_{\text{carb}}$  values (Long, 1993; Finney et al., 1999; Brenchley et al., 2003; Bergström et al., 2006). Although differences occur in absolute magnitudes of the Hirnantian  $\delta^{13}\text{C}_{\text{carb}}$  and  $\delta^{13}\text{C}_{\text{org}}$  shifts, these probably reflect various epeiric sea water masses of flooded landmasses, such as in the case of the early Katian positive  $\delta^{13}\text{C}$  shift (GICE; Young et al., 2005). Upper Ordovician water masses have been previously shown to vary in critical parameters (i.e., nutrient concentrations) that affect growth rates, algal ecology, and ultimately  $\delta^{13}\text{C}$  values (e.g., Holmden et al., 1998; Panchuk et al., 2006; Young et al., 2008). Despite the challenges for precise independent biostratigraphic correlation of the Estonian and Anticosti Island sequences with other latest Ordovician sections worldwide (see above; Section 2), the most parsimonious explanation for the large positive shifts in both  $\delta^{13}\text{C}_{\text{carb}}$  and  $\delta^{13}\text{C}_{\text{org}}$  is that they represent the same perturbation of the global carbon cycle (Fig. 7).



**Table 2**  
Stable isotope data, Kardla Drill Core, Estonia.

Meters	$\delta^{13}\text{C}_{\text{carb}}^a$	$\delta^{18}\text{O}$	$\delta^{13}\text{C}_{\text{org}}$	TOC	Formation	Member	Chitinozoan zone
155.2	0.89	−4.99	−28.52	0.05	Öhne		<i>S. fragilis</i>
157.2	0.92	−4.82	−28.23	0.05	Öhne		<i>S. fragilis</i>
158.2	0.82	−4.68	−28.93	0.08	Öhne		<i>S. fragilis</i>
159.2	0.78	−5.47	−29.09	0.04	Öhne		<i>S. fragilis</i>
160.2	0.70	−4.73	−27.60	0.04	Öhne		<i>S. fragilis</i>
161.0	2.10	−4.10	−27.86	0.06	Öhne		<i>S. fragilis</i>
161.2	4.60	−4.70	−26.68	0.02	Saldus		???
162.0	5.30	−5.30	−26.51	0.02	Saldus		???
163.0	5.80	−4.90	−26.77	0.02	Saldus		???
164.0	5.60	−5.00	−26.25	0.02	Saldus		???
165.0	5.60	−5.10	−26.46	0.02	Saldus		???
166.0	5.40	−4.80	−26.28	0.02	Saldus		???
167.0	6.00	−4.30	−26.72	0.03	Kuldiga	Edole	<i>C. scabra</i>
168.0	6.20	−4.00	−26.37	0.04	Kuldiga	Edole	<i>C. scabra</i>
170.0	6.60	−4.00	−26.15	0.03	Kuldiga	Edole	<i>C. scabra</i>
171.0	6.70	−3.60	−26.42	0.03	Kuldiga	Edole	<i>C. scabra</i>
172.5	6.78	−3.30	−26.28	0.05	Kuldiga	Edole	<i>C. scabra</i>
173.5	6.00	−3.80	−26.17	0.01	Kuldiga	Edole	<i>C. scabra</i>
175.0	6.20	−3.40	−26.02	0.22	Kuldiga	Edole	<i>C. scabra</i>
176.0	3.60	−3.20	−25.43	0.19	Kuldiga	Edole	<i>C. scabra</i>
177.0	3.50	−3.00	−26.03	0.15	Kuldiga	Edole	<i>C. scabra</i>
178.0	4.90	−4.00	−25.48	0.12	Kuldiga	Edole	<i>C. scabra</i>
179.0	5.10	−3.80	−25.79	0.15	Kuldiga	Edole	<i>C. scabra</i>
180.0	4.60	−3.90	−26.36	0.11	Kuldiga	Edole	<i>S. tougourdeani</i>
181.0	3.88	−4.30	−25.94	0.17	Kuldiga	Bernati	<i>S. tougourdeani</i>
181.5	3.49	−4.97	−26.04	0.23	Kuldiga	Bernati	<i>S. tougourdeani</i>
182.0	2.30	−2.90	−27.89	0.11	Kuldiga	Bernati	<i>S. tougourdeani</i>
183.0	2.19	−4.34	−27.90	0.14	Kuldiga	Bernati	<i>S. tougourdeani</i>
184.0	1.90	−3.20	−27.89	0.11	Kuldiga	Bernati	<i>S. tougourdeani</i>
185.0	1.50	−3.20	−28.78	0.12	Kuldiga	Bernati	<i>B. gamachiana</i>
185.5	0.79	−5.29	−28.71	0.12	Halliku		<i>B. gamachiana</i>
187.3	0.76	−4.31	−29.69	0.14	Halliku		<i>C. rugata</i>
188.5	0.78	−4.61	−29.58	0.11	Halliku		<i>C. rugata</i>
190.0	1.10	−3.68	−29.16	0.03	Halliku		<i>C. rugata</i>

<sup>a</sup> Most  $\delta^{13}\text{C}_{\text{carb}}$  values previously reported from Kaljo et al. (2001).

The latest Ordovician sequence from the Monitor Range, Nevada has been the subject of two different stable isotopic studies where separate sections through the Hanson Creek Formation were collected only meters apart from one another (Kump et al., 1999; LaPorte et al., 2009). The  $\delta^{13}\text{C}_{\text{carb}}$  trends from both studies are seemingly identical and compare well with the  $\delta^{13}\text{C}_{\text{carb}}$  values and trends in Estonia. However, organic matter  $\delta^{13}\text{C}_{\text{org}}$  values reported by Kump et al. (1999) are non-trending, whereas LaPorte et al. (2009) document a positive excursion (+4‰) in  $\delta^{13}\text{C}_{\text{org}}$  values. Kump et al. (1999) suggested that the lack of trending  $\delta^{13}\text{C}_{\text{org}}$  data could reflect the relatively high thermal alteration (CAI ~3; >100 °C) compared to other relatively pristine sections (Popp et al., 1998; Hayes et al., 1999) or may reflect possible fluctuations in nutrient delivery that significantly affected phytoplankton growth rates and subsequent  $\delta^{13}\text{C}_{\text{org}}$  values (e.g., modern Peru Upwelling Zone; Bidigare et al., 1997). However, LaPorte et al. (2009) favored a microbial remineralization hypothesis for the Monitor Range, whereby bulk  $\delta^{13}\text{C}_{\text{org}}$  values are lowered by bacterial chemotrophs “re-packaging” algal photosynthate under anoxic bottom waters (Gong and Hollander, 1997). As a result this secondary process may have affected the absolute  $\delta^{13}\text{C}$  values, yet the overall  $\Delta^{13}\text{C}$  trends from both studies (Kump et al., 1999; LaPorte et al., 2009) compare well with Estonia and Anticosti Island (Fig. 8). Paired  $\delta^{13}\text{C}_{\text{carb}}$  and  $\delta^{13}\text{C}_{\text{org}}$  values were also reported from Hirnantian sections at Vinini Creek, Nevada and Blackstone River, Yukon Territory by LaPorte et al. (2009). And it was suggested that the paired trends at Blackstone River faithfully record  $\delta^{13}\text{C}_{\text{DIC}}$ , as the  $\Delta^{13}\text{C}$  values are relatively consistent when compared to the wider ranging  $\Delta^{13}\text{C}$  values from Nevada. Interestingly the same overall trends occur in strata from both Nevada and Yukon Territory sections:  $\Delta^{13}\text{C}$  values trend positively from the *D. mirus* through

*N. extraordinarius* graptolite zones, and  $\Delta^{13}\text{C}$  values decline through *N. persculptus* Zone (Fig. 5 in LaPorte et al., 2009).

Paired  $\delta^{13}\text{C}_{\text{carb}}$  and  $\delta^{13}\text{C}_{\text{org}}$  values have also been reported from latest Ordovician sections in Arctic Canada (Melchin and Holmden, 2006). Although a positive excursion (+3 to +6‰) in  $\delta^{13}\text{C}_{\text{org}}$  values is recorded in Hirnantian strata,  $\delta^{13}\text{C}_{\text{carb}}$  values reported are inconsistent and non-trending from this area. The  $\delta^{13}\text{C}_{\text{carb}}$  values were suggested to be significantly affected by secondary diagenetic processes including: 1) dolomitization, 2) reworking of detrital carbonates from eroded carbonate platforms exposed nearby, and 3) carbonate precipitation from bacterial decomposition of organic matter under sulfate reducing conditions (Coniglio and Melchin, 1995; Melchin and Holmden, 2006). As a result any  $\Delta^{13}\text{C}$  values calculated for these Arctic Canada sections would reflect these diagenetic processes rather than potential changes in carbon cycling during the Hirnantian.

## 5.2. Paired analysis of $\delta^{13}\text{C}_{\text{carb}}$ and $\delta^{13}\text{C}_{\text{org}}$

Although it is possible to interpret the observed changes in  $\Delta^{13}\text{C}$  (Figs. 4 and 5) in many different ways, we believe the most promising interpretation is in relation to changing  $p\text{CO}_2$  and its effects on photosynthetic fractionation. Bulk  $\delta^{13}\text{C}_{\text{org}}$  measurements may contain different algal species with different isotopic fractionations. However, a comparison of bulk organic matter  $\delta^{13}\text{C}_{\text{org}}$  versus source-specific organic molecules in Devonian rocks demonstrated that isotope shifts from both sources are nearly identical in timing and magnitude (Joachimski et al., 2002). A similar study in the Ordovician reported that, despite changes in the relative contribution of an anomalous species that affected  $\delta^{13}\text{C}_{\text{org}}$  locally, the magnitude of the environmental signal was still present and compared well with bulk  $\delta^{13}\text{C}_{\text{org}}$  trends from other regions (Pancost et al., 1999).

Although we still know little about the physiological properties of Ordovician marine algae and the degree to which photoautotroph assemblages may have changed simultaneously in our Estonian and Anticosti Island study areas, it appears cell growth rates should not have changed to produce the observed  $\Delta^{13}\text{C}$  trends. Sedimentary

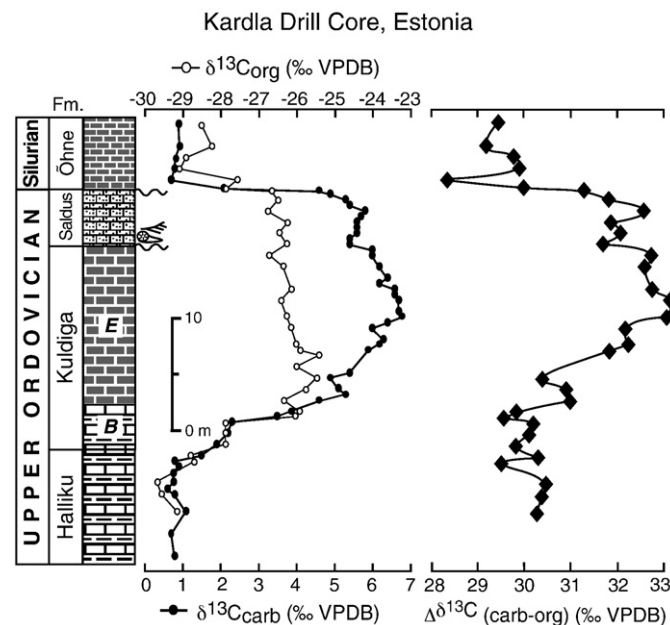


**Fig. 6.** Upper Ordovician to Lower Silurian  $\delta^{13}\text{C}_{\text{carb}}$  and  $\delta^{13}\text{C}_{\text{org}}$  trends for the Kardla drill core, Estonia. B and E, represent the Bernati and Edole members of the Kuldiga Formation. Note that the scales for  $\delta^{13}\text{C}_{\text{carb}}$  and  $\delta^{13}\text{C}_{\text{org}}$  are below and above the data plots, respectively. Additionally, most of the  $\delta^{13}\text{C}_{\text{carb}}$  data is replotted from Kaljo et al. (2001). Also plotted are  $\Delta^{13}\text{C}$  trends, used as a proxy for relative changes in atmospheric  $p\text{CO}_2$ . Note the presence of two unconformities capping the Kuldiga and Saldus formations.

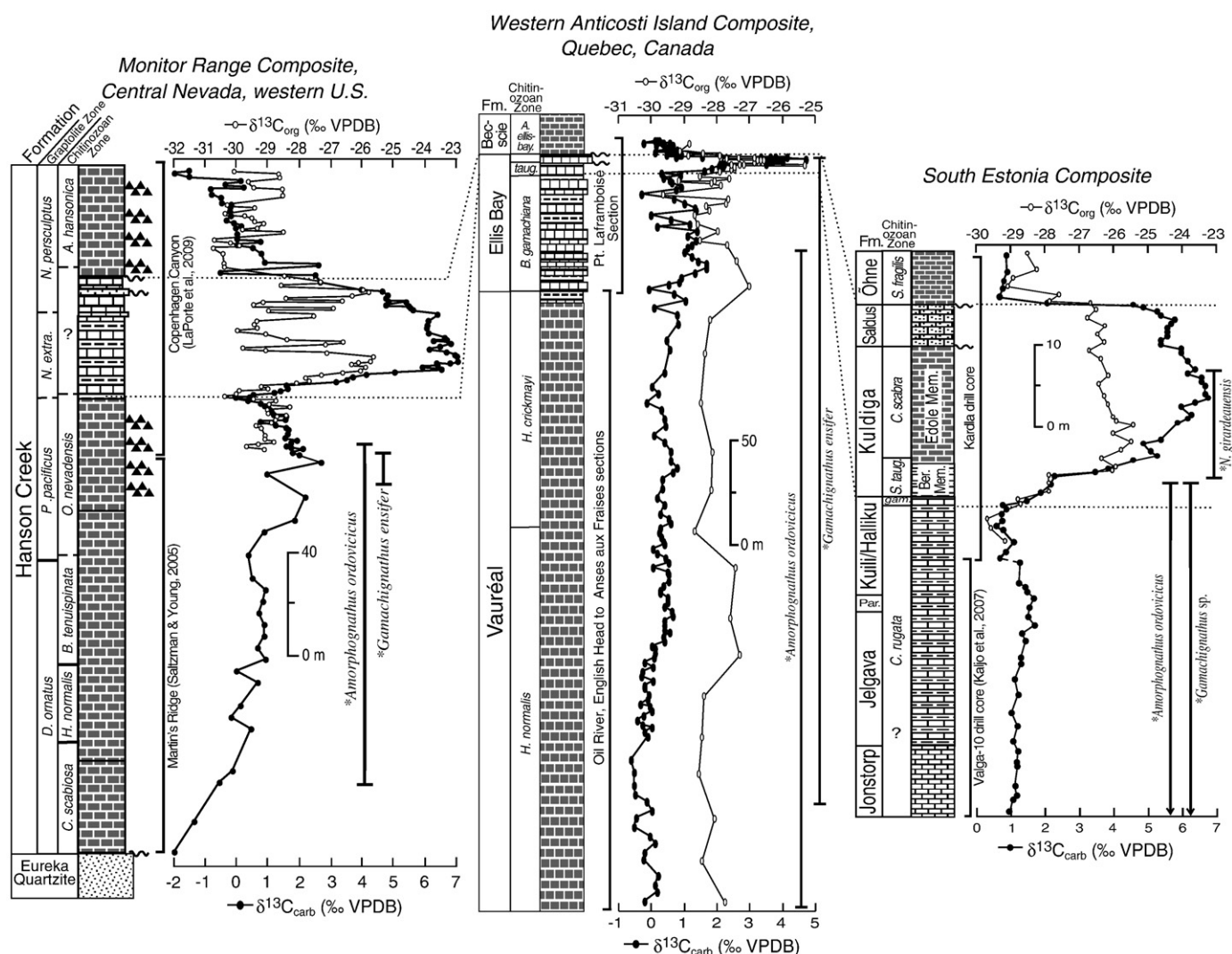


**Fig. 7.** Proposed correlation of paired  $\delta^{13}\text{C}_{\text{carb}}$  and  $\delta^{13}\text{C}_{\text{org}}$  trends from the two Upper Ordovician–Silurian sequences studied here to a previously studied sequence in the Monitor Range, Nevada (Finney et al., 1999; Kump et al., 1999; Saltzman and Young, 2005; LaPorte et al., 2009). Correlation is based on chitinozoan biozones from Estonian Scheme B (see Fig. 3), as this is the most parsimonious (i.e., they all reflect the same perturbation of the global carbon cycle) explanation for the large positive  $\delta^{13}\text{C}_{\text{carb}}$  and  $\delta^{13}\text{C}_{\text{org}}$  excursions documented from these sequences. Chitinozoan biozones and diagnostic conodonts\* are from previous studies (Achab, 1977; Nowlan and Barnes, 1981; McCracken and Nowlan, 1981; Soufine and Achab, 2000; Kaljo et al., 2001; Männik, 2001; Branchley et al., 2003; Kaljo et al., 2008; Achab et al., in press). Please note all composite sections have the same horizontal  $\delta^{13}\text{C}$  scales, but different vertical scales due to varying sedimentation rates in these widely separated paleocean basins. Abbreviations: A. ellisbayensis (A. ellisbay.), S. taugourdeui (taug.), B. gamachiana (gam.), Paroveja Formation (Par.).

indicators of enhanced nutrient delivery (e.g., bedded chert and phosphate; Pope and Steffen, 2003) that would drive phytoplankton growth rates higher (e.g., modern Peru Upwelling Zone; Bidigare et al., 1997) are found in some regions but not in our Estonia or Anticosti Island study sections. It is unlikely that nutrient dynamics changed drastically in these low-latitude, predominantly oligotrophic settings, although sea surface temperatures may have fluctuated.

When  $\text{CO}_2(\text{aq})$  equilibrates with DIC a large, temperature dependent ( $0.12\text{‰}/^\circ\text{C}$ ) isotopic enrichment ( $\sim +8\text{‰}$  to  $+12\text{‰}$ ) takes place (Goericke and Fry, 1994). An 8‰ decline in  $\Delta^{13}\text{C}$  values through the Oligocene to the Pleistocene has been recorded and  $\sim 1\%$  of this drop is attributed to global cooling (Hayes et al., 1999). Although the latest Ordovician sections discussed here were deposited in relatively shallow tropical–subtropical settings, only small temperature fluctuations are expected (see Fig. 2). Sea surface temperatures recently calculated from conodont–apatite  $\delta^{18}\text{O}$  values in a low-latitude marine setting (i.e., Anticosti Island) do show a drop in the Hirnantian ( $\sim 27\text{--}23^\circ\text{C}$ ; Trotter et al., 2008). These temperature fluctuations would only account for  $\sim 0.30\text{--}0.50\text{‰}$  of the 3 to 5‰ shifts in  $\Delta^{13}\text{C}$  values documented from the various Hirnantian sequences discussed here.

Additionally, there is also no evidence for simultaneous changes in the mineralogy of carbonates and  $\delta^{13}\text{C}$  in our study sections that would affect fractionation between DIC and precipitated carbonate minerals. Secondary biological fractionation resulting from heterotrophy and organic matter diagenesis also seem unlikely because of the global nature of the  $\Delta^{13}\text{C}$  trends (Fig. 8) (Hayes et al., 1999).

The observed change in  $\Delta^{13}\text{C}$  through the Hirnantian Stage in Estonia and Anticosti Island can be interpreted to reflect atmospheric  $p\text{CO}_2$  levels that were relatively low immediately prior to the  $\delta^{13}\text{C}_{\text{carb}}$  excursion and then increased as ice sheets expanded (Figs. 5 and 6). Ultimately, this period of elevated  $p\text{CO}_2$  is followed by global deglaciation. The timing of the changes in  $\Delta^{13}\text{C}$  and ice volume (inferred from sea-level reconstructions) is consistent with biostratigraphic and  $\delta^{13}\text{C}_{\text{carb}}$  evidence that links major erosional surfaces in low-latitude carbonate platforms from Midcontinent North America and Europe to the timing of tillite deposition on Gondwana (Bergström et al., 2006). In North Africa (Gondwana), major tillite deposits are separated by Hirnantian sequences of deltaic, estuarine, or fluvial sediments interpreted to reflect an interglacial highstand (e.g., Sutcliffe et al., 2000; Ghiene, 2003).

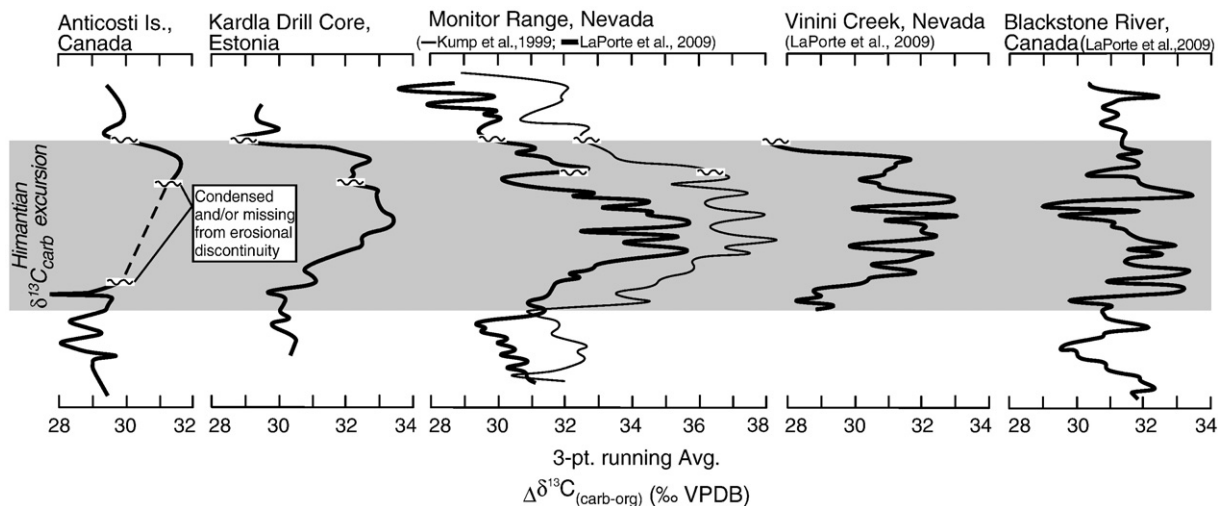


**Fig. 8.** Comparison of  $\Delta^{13}\text{C}$  three-point running average curves from Anticosti Island, Canada and Estonia to previously studied sections from Nevada and Yukon Territory, Canada (Kump et al., 1999; LaPorte et al., 2009). Correlation is based on chitinozoan biozones from Estonian Scheme B (see Fig. 3), as this is the most parsimonious (i.e., they all reflect the same perturbation of the global carbon cycle) explanation for the large positive  $\delta^{13}\text{C}_{\text{carb}}$  and  $\delta^{13}\text{C}_{\text{org}}$  excursions documented from these sequences.  $\Delta^{13}\text{C}$  curves from these sections have been scaled respectively to conform to the area of the Hirnantian  $\delta^{13}\text{C}_{\text{carb}}$  excursion (grey rectangle). Note that the grey rectangle indicates where  $\delta^{13}\text{C}_{\text{carb}}$  values deviate positively from a baseline and later return to baseline values in all sections.

### 5.3. Timing of the latest Ordovician glaciation

On Anticosti Island, evidence for Hirnantian ice volume expansion is based on a major coarsening upward cycle (Long, 1993, 2007) through the upper Lousy Cove Member of the Ellis Bay Formation (Fig. 5). The shallowing is marked by deposition of calcareous shale and lime mudstone passing gradually upward into skeletal wack-

estone/packstone with shale interbeds that are overlain by locally cross-bedded skeletal to peloidal packstones/grainstones (Desrochers et al., 2010-this issue). The abrupt contact with the overlying Laframboise Member is erosional (Long, 2007; Desrochers et al., 2010-this issue) and represents maximum ice volume. The oncolite and reefal carbonates that record the peak of the  $\delta^{13}\text{C}_{\text{carb}}$  excursion in the Laframboise Member were likely deposited during an interglacial

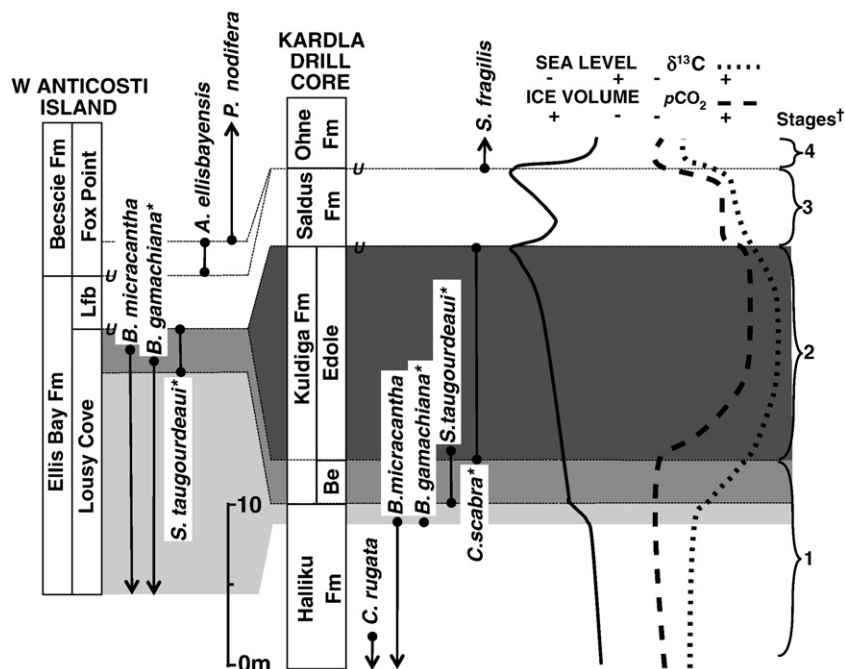


**Fig. 9.** Correlation of Upper Ordovician to Lower Silurian strata,  $\delta^{13}\text{C}$  curves, sea level, inferred ice volume, and  $p\text{CO}_2$  trends from Estonia to western Anticosti Island, Quebec. Diagnostic chitinozoan species are plotted along with important zones\* (*B. gamachiana* and *S. taugourdeui* zones; light and medium grey shaded intervals) previously reported from these sections (Soufiane and Achab, 2000; Brenchley et al., 2003; Achab et al., in press; Desrochers et al., this issue). The dark grey interval from the Kardla drill core represents the *C. scabra* chitinozoan zone, and this interval is likely missing at an unconformity (U) at the base of the Laframboise Member in the Point Laframboise section (Long, 2007; Desrochers et al., this issue). Due to the lack of biostratigraphically useful fossils found in the Laframboise Member and Saldus Formation, their correlation is tentative and based upon biostratigraphy of the underlying and overlying strata, similar  $\delta^{13}\text{C}$  values, and comparable carbonate facies and sea-level histories. The inferred Gondwana (North Africa) ice volume curve is after previously reported sea-level curves from both study sections (Brenchley et al., 2003; Desrochers et al., this issue). Stages<sup>†</sup>: (1) sedimentary shallowing upward trends,  $\delta^{13}\text{C}_{\text{carb}}$  and  $\delta^{13}\text{C}_{\text{org}}$  values are low and then begin rising,  $p\text{CO}_2$  levels are low, development of ice sheets; (2) continuation of shallowing upward trends, maximum  $\delta^{13}\text{C}_{\text{carb}}$  and  $\delta^{13}\text{C}_{\text{org}}$  values,  $p\text{CO}_2$  levels rise and reach maximum, further expansion of ice sheets, and reduction of continental silicates for weathering; (3) Initial deepening followed by shallowing upward trends, high  $\delta^{13}\text{C}_{\text{carb}}$ ,  $\delta^{13}\text{C}_{\text{org}}$ , and  $p\text{CO}_2$  levels, interglacial episode followed by renewed expansion of ice sheets; (4) deepening upward trends, low  $\delta^{13}\text{C}_{\text{carb}}$ ,  $\delta^{13}\text{C}_{\text{org}}$ , and  $p\text{CO}_2$  levels, ice sheets collapse, and continental silicates are available for weathering. Lfb and Be, represent the Laframboise and Bernati members.



highstand (Desrochers et al., 2010-this issue). The abrupt contact with the overlying Becscie Formation Member is also erosional (Long, 2007; Desrochers et al., 2010-this issue) indicating a second glacial maximum. This sea-level interpretation on Anticosti Island is mirrored in the timing of facies changes and unconformities as recorded in Estonia (Kaljo et al., 2001; Branchley et al., 2003) (Fig. 6).

In South Estonia, the transition in the Kuldiga Formation from more argillaceous lime mudstones and wackestones (Bernati Member) to skeletal wackestones interbedded with admixtures of marl, silt, and sand (Edole Member; records peak  $\delta^{13}\text{C}_{\text{carb}}$  values) signals a major sea-level drop (Kaljo et al., 2001). The disconformity at the top of the Kuldiga Formation likely represents a glacial maximum. A relative rise in sea level is recorded by the oolitic/skeletal packstones and grainstones of the overlying Saldus Formation (Branchley et al., 2003). The top of the Saldus Formation is capped by a second, more extensive disconformity, likely representing a second glacial maximum.

The Hanson Creek Formation, Nevada contains sedimentary indicators of upwelling associated with cooling (e.g., chert and phosphate; Pope and Steffen, 2003) that precede the  $\delta^{13}\text{C}_{\text{carb}}$  excursion, and are overlain by a shallowing upward sea-level history (Finney et al., 1999; Kump et al., 1999) consistent with that described for Anticosti Island and Estonia. Matching Hirnantian shallowing upward cycles, erosional surfaces, and oolitic/skeletal carbonates deposited during an interglacial occur in carbonates from the North American Midcontinent (Orchard Creek, Girardeau, and Leemon formations) that record the Hirnantian  $\delta^{13}\text{C}_{\text{carb}}$  excursion (Bergström et al., 2006).

One potential challenge to an interglacial highstand model for the Hirnantian  $\delta^{13}\text{C}_{\text{carb}}$  excursion is that a coincident positive shift in  $\delta^{18}\text{O}$  has also been documented (Branchley et al., 1994; 2003) (see also Tables 1 and 2). This  $\delta^{18}\text{O}$  shift has been attributed to lowered sea surface temperatures and ice volume changes (Branchley et al., 1994). If this previously documented  $\sim +2\text{--}3\text{‰}$  shift in  $\delta^{18}\text{O}$  were only interpreted as a paleotemperature indicator, it would correspond to a change of  $\sim 10\text{--}12\text{ °C}$  in shallow tropical seas. However, Hirnantian sea surface temperatures calculated from conodont-apatite  $\delta^{18}\text{O}$  values in low-latitude marine setting reveal a smaller decline ( $\sim 4\text{ °C}$ ) in temperature (Trotter et al., 2008; see also Fig. 1). This recent Ordovician finding is similar to temperature variations in tropical seas during the last glacial–interglacial transition (late Quaternary) that only varied by  $1\text{--}2\text{ °C}$  (CLIMAP, 1981). Marine  $\delta^{18}\text{O}$  values are also sensitive to evaporation and precipitation in surface waters and the mixing of water masses containing differing  $^{18}\text{O}/^{16}\text{O}$  ratios (e.g., glacial melt waters, river runoff). A model developed for Silurian positive  $\delta^{18}\text{O}$  shifts (Bickert et al., 1997) suggests these trends are more likely records of paleosalinity than paleotemperature. Paleosalinity ranges of 32.5‰ to 38.0‰ calculated from Silurian positive  $\delta^{18}\text{O}$  shifts (comparable in magnitude and timing to the Hirnantian  $\delta^{18}\text{O}$  shift) are consistent with modern surface ocean salinity ranges (Bickert et al., 1997). The Hirnantian skeletal and reefal carbonates that record high  $\delta^{13}\text{C}$  and  $\delta^{18}\text{O}$  values deposited during an interglacial highstand are consistent with the carbonate facies, oceanic circulation, and arid low-latitude climatic conditions predicted by the Bickert et al. (1997) salinity model.

## 6. Implications and conclusions

Our data are consistent with the notion that a long-term drop in  $p\text{CO}_2$  due to increased silicate weathering (Kump et al., 1999; Saltzman and Young, 2005; Young et al., 2009) possibly also combined with reduced poleward ocean heat transport (Herrmann et al., 2004) resulted in the initial stage of glaciation beginning prior to Stage 1 in Fig. 9. As expanding ice sheets reduced the fraction of continental silicates available for weathering,  $p\text{CO}_2$  began to rise and  $\delta^{13}\text{C}_{\text{carb}}$  continued to increase due to carbonate weathering in low to mid latitudes (Stage 2 in Fig. 9). The elevated  $p\text{CO}_2$  levels eventually led to

deglaciation, as recorded by the rapid transgression above an unconformity in both Estonia and Anticosti Island (start of Stage 3 in Fig. 6). Following deglaciation, renewed silicate weathering (possibly supplemented by enhanced burial of organic matter in the deepening oceans) led to a second draw down in  $p\text{CO}_2$  levels and a final episode of Hirnantian glacial advance (end of Stage 3). Organic matter burial or enhanced preservation  $\text{C}_{\text{org}}$  in the deep oceans through much of Hirnantian is supported by recent documentation of a large positive excursion ( $+10\text{--}20\text{‰}$ ) in  $\delta^{34}\text{S}$  of pyrites that tracks the positive  $\delta^{13}\text{C}_{\text{org}}$  excursion potentially resulting from both isotopically light carbon ( $^{12}\text{C}$ ) and sulfur ( $^{32}\text{S}$ ) being sequestered in deeper anoxic waters during the Hirnantian (Zhang et al., 2009). However, further studies of  $\delta^{34}\text{S}$  of carbonate-associated sulfates are needed to determine if the Hirnantian seawater sulfate reservoir became enriched in  $^{34}\text{S}$  as a result of anoxic deep waters. The resultant second episode of glaciation was short lived and deglaciation may also have been related to changes in  $p\text{CO}_2$  levels, but the available data are not at high enough resolution to determine this.

## Acknowledgements

We thank P. Copper, J. Richardson, S. Bergström, S. Leslie, B. Cramer, C. Holmden, T. Prokopiuk, K. Foland, J. Linder, Y. Matsui, and A. Grotoli for their help with fieldwork, useful discussions, and/or use of laboratory facilities. This manuscript has benefited from careful and detailed reviews by M. Melchin, A. Munnecke, and an anonymous reviewer. This research was supported by grants from the National Geographic Society (67-89-00), the National Science Foundation (EAR 0125249) to W.I. Ausich and M.R. Saltzman, the Canadian Discovery Grant (17885) to A. Desrochers, and Estonian target project SF 0140020s08 to D. Kaljo. Additional funding came from student grants to S.A. Young from the Ohio State University and GSA. We also thank the Estonian Geological Survey for permission to study the Kardla drill core. This study is a contribution to IGCP project No. 503.

## References

- Achab, A., 1977. Les chitinozoaires de la zone à *Climacograptus prominens elongatus*, de la Formation de Vauréal (Ordovicien supérieur), Ile d'Anticosti, Québec. Canadian Journal of Earth Sciences 14, 2193–2212.
- Achab, A., Asselin, E., Desrochers, A., Riva, J., Farley, C., in press. Chitinozoan biostratigraphy of a new Upper Ordovician Stratigraphic framework for Anticosti Island, Canada. Geological Society of America Bulletin.
- Banner, J.L., Hanson, G.N., 1990. Calculation of simultaneous isotopic and trace element variations during water–rock interaction with applications to carbonate diagenesis. *Geochimica et Cosmochimica Acta* 54, 3123–3137.
- Bergström, S.M., Saltzman, M.R., Schmitz, B., 2006. First record of the Hirnantian (Upper Ordovician)  $\delta^{13}\text{C}$  excursion in the North American Midcontinent and its regional implications. *Geological Magazine* 143, 657–678.
- Bickert, T., Pätzold, J., Samtleben, C., Munnecke, A., 1997. Paleoenvironmental changes in the Silurian indicated by stable isotopes in brachiopods from Gotland, Sweden. *Geochimica et Cosmochimica Acta* 61, 2717–2730.
- Bigdare, R.R., Fluegge, A., Freeman, K.H., Hanson, K.L., Hayes, J.M., Hollander, D., Jasper, J.P., King, L.L., Laws, E.A., Milder, J., Millero, F.J., Pancost, R., Popp, B.N., Steinberg, P.A., Wakeham, S.G., 1997. Consistent fractionation of  $^{13}\text{C}$  in nature and in the laboratory: growth-rate effects in some haptophyte algae. *Global Biogeochemical Cycles* 11, 279–292.
- Branchley, P.J., Marshall, J.D., Carden, G.A.F., Robertson, D.B.R., Long, D.G.F., Meidla, T., Hints, L., Anderson, T.F., 1994. Bathymetric and isotopic evidence for a short-lived Late Ordovician glaciation in a greenhouse period. *Geology* 22, 295–298.
- Branchley, P.J., Carden, G.A.F., Marshall, J.D., 1995. Environmental changes associated with the “first strike” of the Late Ordovician mass extinction. *Modern Geology* 20, 69–82.
- Branchley, P.J., Carden, G.A.F., Hints, L., Kaljo, D., Marshall, J.D., Martma, T., Meidla, T., Nolvak, J., 2003. High-resolution stable isotope stratigraphy of Upper Ordovician sequences: constraints on the timing of bioevents and environmental changes associated with mass extinction and glaciation. *Geological Society of America Bulletin* 115, 89–104.
- Chen, X., Rong, J.-Y., Fan, J.-X., Zhan, R.-B., Mitchell, C.E., Harper, D.A.T., Melchin, M.J., Peng, P.-A., Finney, S.C., Wang, X.-F., 2006. The Global Stratotype Section and Point (GSSP) for the base of the Hirnantian Stage (the uppermost of the Ordovician System). *Episodes* 29, 183–196.
- CLIMAP Project Members, 1981. Seasonal reconstruction of the Earth's surface at the last glacial maximum. Geological Society of America Map & Chart Series, MC-36.



- Cocks, L.R.M., Torsvik, T.H., 2002. Earth geography from 500 to 400 million years ago: a faunal and paleomagnetic review. *Journal of the Geological Society, London* 159, 631–644.
- Coniglio, M., Melchin, M., 1995. Petrography and isotope geochemistry of diagenetic carbonates in the later Cape Phillips Formation, Cornwallis Island, Arctic Archipelago, Canada. *Bulletin of Canadian Petroleum Geology* 43, 251–266.
- Copper, P., 2001. Reefs during the multiple crises towards the Ordovician–Silurian boundary: Anticosti Island, eastern Canada, and worldwide. *Canadian Journal of Earth Sciences* 38, 153–171.
- Delabroye, A., Vecoli, M., 2010. The end-Ordovician glaciation and the Hirnantian Stage: a global review and questions about the Late Ordovician event stratigraphy. *Earth-Science Reviews* 98, 269–282. doi:10.1016/j.earscirev.2009.10.010.
- Desrochers, A., Farley, F., Achab, A., Asselin, E., Riva, J., 2010. A far-field record of the end Ordovician glaciation: The Ellis Bay Formation, Anticosti Island, Eastern Canada. *Palaeogeography, Palaeoclimatology, Palaeoecology* 296, 248–263 (this issue).
- Finney, S.C., Berry, W.B.N., Cooper, J.D., Ripperdan, R.L., Sweet, W.C., Jacobson, S.R., Soufiane, A., Achab, A., Noble, P.J., 1999. Late Ordovician mass extinction: a new perspective from stratigraphic sections in central Nevada. *Geology* 27, 215–218.
- Francois, R., Altabet, M.A., Goericke, R., McCorkle, D.C., Brunet, C., Poisson, A., 1993. Changes in the  $\delta^{13}\text{C}$  of surface water particulate organic matter across the subtropical convergence in the SW Indian Ocean. *Global Biogeochemical Cycles* 7, 627–644.
- Gao, G., Dworkin, S.L., Land, L.S., Elmore, R.D., 1996. Geochemistry of Late Ordovician Viola Limestone, Oklahoma: implications for marine carbonate mineralogy and isotopic compositions. *Journal of Geology* 104, 359–367.
- Ghienne, J., 2003. Late Ordovician sedimentary environments, glacial cycles, and post-glacial transgression in the Taoudeni Basin, West Africa. *Palaeogeography, Palaeoclimatology, Palaeoecology* 189, 117–145.
- Goericke, R., Fry, B., 1994. Variations of marine plankton  $\delta^{13}\text{C}$  with latitude, temperature, and dissolved  $\text{CO}_2$  in the world ocean. *Global Biogeochemical Cycles* 8, 85–90.
- Gong, C., Hollander, D.J., 1997. Differential contribution of bacteria to sedimentary organic matter in oxic and anoxic environments, Santa Monica Basin, California. *Organic Geochemistry* 26, 545–563.
- Harper, D.A.T., Rong, J.-Y., 2008. Completeness of the Hirnantian brachiopod record: spatial heterogeneity through the end Ordovician extinction event. *Lethia* 41, 195–197.
- Hayes, J.M., Strauss, H., Kaufman, A.J., 1999. The abundance of  $^{13}\text{C}$  in marine organic matter and isotopic fractionation in the global biogeochemical cycle of carbon during the past 800 Ma. *Chemical Geology* 161, 103–125.
- Herrmann, A.D., Haupt, B.J., Patzkowsky, M.E., Seidov, D., Slingerland, R.L., 2004. Response of Late Ordovician paleoceanography to changes in sea level, continental drift, and atmospheric  $\text{pCO}_2$ : potential causes for long-term cooling and glaciation. *Palaeogeography, Palaeoclimatology, Palaeoecology* 210, 385–401.
- Holmden, C., Creaser, R.A., Muehlenbachs, K., Leslie, S.A., Bergström, S.M., 1998. Isotopic evidence for geochemical decoupling between ancient epicritic seas and bordering oceans: implications for secular curves. *Geology* 26, 567–570.
- Jin, J., Copper, P., 1997. *Parastrophinella* (Brachiopoda): its paleogeographic significance at the Ordovician/Silurian boundary. *Journal of Paleontology* 71, 369–380.
- Jin, J., Copper, P., 2008. Response of brachiopod communities to environmental change during the Late Ordovician mass extinction interval, Anticosti Island, Eastern Canada. *Fossils and Strata* 54, 41–51.
- Joachimski, M.M., Pancost, R.D., Freeman, K.H., Ostertag-Henning, C., Buggisch, W., 2002. Carbon isotope geochemistry of the Frasnian–Famennian transition. *Palaeogeography, Palaeoclimatology, Palaeoecology* 181, 91–109.
- Kaljo, D., Hints, L., Martma, T., Nölvak, J., 2001. Carbon isotope stratigraphy in the latest Ordovician of Estonia. *Chemical Geology* 175, 49–59.
- Kaljo, D., Martma, T., Saadre, T., 2007. Post-Hunnebergian Ordovician carbon isotope trend in Baltoscandia, its environmental implications and some similarities with that of Nevada. *Palaeogeography, Palaeoclimatology, Palaeoecology* 245, 138–155.
- Kaljo, D., Hints, L., Männik, P., Nölvak, J., 2008. The succession of Hirnantian events based on data from Baltica: brachiopods, chitinozoans, conodonts, and carbon isotopes. *Estonian Journal of Earth Sciences* 57, 197–218.
- Kump, L.R., Arthur, M.A., 1999. Interpreting carbon-isotope excursions: carbonates and organic matter. *Chemical Geology* 161, 181–198.
- Kump, L.R., Arthur, M.A., Patzkowsky, M.E., Gibbs, M.T., Pinkus, D.S., Sheehan, P.M., 1999. A weathering hypothesis for glaciation at high atmospheric  $\text{pCO}_2$  during the Late Ordovician. *Palaeogeography, Palaeoclimatology, Palaeoecology* 152, 173–187.
- LaPorte, D.F., Holmden, C., Patterson, W.P., Loxton, J.D., Melchin, M.J., Mitchell, C.E., Finney, S.C., Sheets, H.D., 2009. Local and global perspectives on carbon and nitrogen cycling during the Hirnantian Glaciation. *Palaeogeography, Palaeoclimatology, Palaeoecology* 276, 182–195. doi:10.1016/j.palaeo.2009.03.009.
- Long, D.G.F., 1993. Oxygen and carbon isotopes and event stratigraphy near the Ordovician–Silurian boundary, Anticosti Island, Quebec. *Palaeogeography, Palaeoclimatology, Palaeoecology* 104, 49–59.
- Long, D.G.F., 2007. Tempestite frequency curves: a key to Late Ordovician and Early Silurian subsidence, sea-level change, and orbital forcing in the Anticosti foreland basin, Quebec, Canada. *Canadian Journal of Earth Sciences* 44, 413–431.
- Männik, P., 2001. Distribution of conodonts. In: Pöldre, A. (Ed.), *Estonia Geological Sections Valga (10) Drill Core: Geological Survey of Estonia Bulletin*, 3, pp. 10–12.
- McCracken, A.D., Barnes, C.R., 1981. Conodont biostratigraphy and paleoecology of the Ellis Bay Formation, Anticosti Island, Quebec, with special reference to Late Ordovician–Early Silurian chronostratigraphy and the systemic boundary. *Geological Survey of Canada Bulletin* 329, 51–126.
- McCracken, A.D., Nowlan, G.S., 1986. The Gamachian Stage and Fauna 13. New York State Museum Bulletin 462, 71–79.
- Melchin, M.J., 2008. Restudy of some Ordovician–Silurian boundary graptolites from Anticosti Island, Canada, and their biostratigraphic significance. *Lethia* 41, 155–162.
- Melchin, M.J., Holmden, C., 2006. Carbon isotope chemostratigraphy in Arctic Canada: Sea-level forcing of carbonate platform weathering and implications for Hirnantian global correlation. *Palaeogeography, Palaeoclimatology, Palaeoecology* 234, 186–200.
- Melchin, M.J., Holmden, C., Williams, S.H., 2003. Correlation of graptolite biozones, chitinozoan biozones, and carbon isotope curves through the Hirnantian. In: Albanesi, G.L., Beresi, M.S., Peralta, S.H. (Eds.), *Ordovician from the Andes: INSUGEO, serie Correlación Geológica*, 17, pp. 101–104.
- Nölvak, J., Hints, O., Mannik, P., 2006. Ordovician timescale in Estonia; recent developments. *Proceedings of the Estonian Academy of Sciences, Geology=Eesti Teaduste Akadeemia Toimetised. Geologia* 55, 95–108.
- Nowlan, G., Barnes, C.R., 1981. Late Ordovician conodonts from the Vaureal Formation, Anticosti Island, Quebec. *Geological Survey of Canada Bulletin* 329, 1–49.
- Panchuk, K.M., Holmden, C.M., Leslie, S.A., 2006. Local controls on carbon cycling in the Ordovician midcontinent region of North America, with implications for carbon isotope secular curves. *Journal of Sedimentary Research* 76, 200–211.
- Pancost, R.D., Freeman, K.H., Patzkowsky, M.E., 1999. Organic-matter source variation and the expression of a late Middle Ordovician carbon isotope excursion. *Geology* 27, 1015–1018.
- Patzkowsky, M.E., Slupik, L.M., Arthur, M.A., Pancost, R.D., Freeman, K.H., 1997. Late Middle Ordovician environmental change and extinction: harbinger of the Late Ordovician or continuation of Cambrian patterns? *Geology* 25, 911–914.
- Pope, M.C., Steffen, J.B., 2003. Widespread, prolonged late Middle to Late Ordovician upwelling in North America: a proxy record of glaciation? *Geology* 31, 63–66.
- Popp, B.N., Laws, E.A., Bidigare, R.R., Dore, J.E., Hanson, K.L., Wakeham, S.G., 1998. Effect of phytoplankton cell geometry on carbon isotopic fractionation. *Geochimica et Cosmochimica Acta* 62, 69–77.
- Riva, J., 1988. Graptolites at and below the Ordovician–Silurian boundary on Anticosti Island, Canada. *Bulletin of the British Museum, Natural History. Geology Series* 43, 221–237.
- Rong, J.-Y., Harper, D.A.T., 1988. A global synthesis of the latest Ordovician Hirnantian brachiopod faunas. *Transactions of the Royal Society of Edinburgh, Earth Sciences* 79, 383–402.
- Rong, J.-Y., Chen, X., Harper, D.A.T., 2002. The latest Ordovician Hirnantian Fauna (Brachiopoda) in time and space. *Lethia* 35, 213–249.
- Saltzman, M.R., 2002. Carbon isotope ( $\delta^{13}\text{C}$ ) stratigraphy across the Silurian–Devonian transition in North America: evidence for a perturbation of the global carbon cycle. *Palaeogeography, Palaeoclimatology, Palaeoecology* 187, 83–100.
- Saltzman, M.R., 2005. Phosphorus, nitrogen, and the redox evolution of the Paleozoic oceans. *Geology* 33, 573–576.
- Saltzman, M.R., Young, S.A., 2005. A long-lived glaciation in the Late Ordovician?: isotopic and sequence-stratigraphic evidence from western Laurentia. *Geology* 33, 109–112.
- Saltzman, M.R., Brasier, M.D., Ripperdan, R.L., Ergaliev, G.K., Lohmann, K.C., Robinson, R.A., Chang, W.T., Peng, S., Runnegar, B., 2000. A global carbon isotope excursion (SPICE) during the Late Cambrian: relation to trilobite extinctions. *Palaeogeography, Palaeoclimatology, Palaeoecology* 162, 211–223.
- Sheehan, P.M., 2001. The Late Ordovician mass extinction. *Annual Review of Earth and Planetary Sciences* 29, 331–364. doi:10.1146/annurev.earth.29.1.331.
- Soufiane, A., Achab, A., 2000. Chitinozoan zonation of the Late Ordovician and the Early Silurian of the island of Anticosti, Quebec, Canada. *Review of Palaeobotany and Palynology* 109, 85–111.
- Soufiane, A., Achab, A., 2000. Upper Ordovician and Lower Silurian chitinozoans from central Nevada and Arctic Canada. *Review of Palaeobotany and Palynology* 113, 165–187.
- Sutcliffe, O.E., Dowdeswell, J.A., Whittington, R.J., Theron, J.N., Craig, J., 2000. Calibrating the Late Ordovician glaciation and mass extinction by the eccentricity cycles of Earth's orbit. *Geology* 28, 967–970.
- Trotter, J.A., Williams, I.A., Barnes, C.R., Lécuyer, C., Nicoll, R.S., 2008. Did cooling oceans trigger Ordovician Biodiversification? Evidence from conodont thermometry. *Science* 321, 550–554.
- Underwood, C.J., Crowley, S.F., Marshall, J.D., Brenchley, P.J., 1997. High-resolution carbon isotope stratigraphy of the basal Silurian Stratotype (Dob's Linn, Scotland) and its global correlation. *Journal of the Geological Society, London* 154, 709–718.
- Vandenbroucke, T.R.A., 2008. An Upper Ordovician chitinozoan biozonation in British Avalonia (England and Wales). *Lethia* 41, 275–294.
- Wang, K., Chatterton, B.D.E., Wang, Y., 1997. An organic carbon isotope record of Late Ordovician to Early Silurian marine sedimentary rocks, Yangtze Sea, South China: implications for  $\text{CO}_2$  changes during the Hirnantian glaciation. *Palaeogeography, Palaeoclimatology, Palaeoecology* 132, 147–158.
- Webby, B.D., Paris, F., Droser, M.L., Percival, I.G., 2004. The Great Ordovician Biodiversification Event. Columbia Press, New York.
- Yapp, C.J., Poths, H., 1992. Ancient atmospheric  $\text{CO}_2$  pressures inferred from natural goethites. *Nature* 355, 342–344.
- Young, S.A., Saltzman, M.R., Bergström, S.M., 2005. Upper Ordovician (Mohawkian) carbon isotope ( $\delta^{13}\text{C}$ ) stratigraphy in eastern and central North America: Regional expression of a perturbation of the global carbon cycle. *Palaeogeography, Palaeoclimatology, Palaeoecology* 222, 53–76.
- Young, S.A., Saltzman, M.R., Bergström, S.M., Leslie, S.A., Chen, X., 2008. Paired  $\delta^{13}\text{C}_{\text{carb}}$  and  $\delta^{13}\text{C}_{\text{org}}$  records of Upper Ordovician (Sandbian–Katian) carbonates in North America and China: implications for paleoceanographic change. *Palaeogeography, Palaeoclimatology, Palaeoecology* 270, 166–178.
- Young, S.A., Saltzman, M.R., Folland, K.A., Linder, J.S., Kump, L.R., 2009. A major drop in seawater  $^{87}\text{Sr}/^{86}\text{Sr}$  during the Middle Ordovician (Darrivilian): links to volcanism and climate? *Geology* 37, 951–954.
- Zhang, T., Shen, Y., Zhan, R., Shen, S., Chen, X., 2009. Large perturbations of the carbon and sulfur cycle associated with the Late Ordovician mass extinction in South China. *Geology* 37, 299–302.